

# A Survey on STT-MRAM Testing: Failure Mechanisms, Fault Models, and Tests

Lizhou Wu<sup>1</sup> Mottaqiallah Taouil<sup>1</sup> Siddharth Rao<sup>2</sup> Erik Jan Marinissen<sup>2</sup> Said Hamdioui<sup>1</sup>  
<sup>1</sup>Delft University of Technology <sup>2</sup>IMEC  
 Mekelweg 4, 2628 CD Delft, The Netherlands Kapeldreef 75, B-3001 Leuven, Belgium  
 {Lizhou.Wu, M.Taouil, S.Hamdioui}@tudelft.nl {Siddharth.Rao, Erik.Jan.Marinissen}@imec.be

As one of the most promising emerging non-volatile memory (NVM) technologies, spin-transfer torque magnetic random access memory (STT-MRAM) has attracted significant research attention due to several features such as high density, zero standby leakage, and nearly unlimited endurance. However, a high-quality test solution is required prior to the commercialization of STT-MRAM. In this paper, we present all STT-MRAM failure mechanisms: manufacturing defects, extreme process variations, magnetic coupling, STT-switching stochasticity, and thermal fluctuation. The resultant fault models including permanent faults and transient faults are classified and discussed. Moreover, the limited test algorithms and design-for-testability (DfT) designs proposed in the literature are also covered. It is clear that test solutions for STT-MRAMs are far from well established yet, especially when considering a defective part per billion (DPPB) level requirement. We present the main challenges on the STT-MRAM testing topic at three levels: failure mechanisms, fault modeling, and test/DfT designs.

**Index Terms**—STT-MRAM Testing, Failure Mechanisms, Manufacturing Defects, Fault Models, Test Algorithms, DfT Designs

## I. INTRODUCTION

Technology downscaling has driven a great success of the semiconductor industry in delivering faster, cheaper, and denser charge-based memories such as SRAM, DRAM, and Flash. However, as these existing memory technologies approach their scaling limits, they become increasingly power hungry and less reliable while the fabrication is more expensive due to the increased manufacturing complexity [1]. As alternative solutions, several promising non-volatile memory (NVM) technologies have emerged and attracted extensive R&D attentions for various levels in the memory hierarchy [2–4]. Among them, spin-transfer torque magnetic random access memory (STT-MRAM) is considered as the leading candidate to replace SRAM for last-level caches (LLCs) in the short term and may serve as a universal memory technology in the long run [5]. The most attractive features of STT-MRAM, compared to SRAM and DRAM, are its non-volatility and nearly zero leakage power. The performance of STT-MRAM is customizable to the target application by having a trade-off between write latency and retention time [6]. Moreover, STT-MRAM offers an integration density ( $6\text{--}20\text{ F}^2$ ) as high as DRAM ( $6\text{--}10\text{ F}^2$ ) [7], essentially unlimited endurance ( $>10^{15}$  cycles) [8], and CMOS-compatibility. Thanks to these attractive advantages, many companies worldwide have been heavily investing in the commercialization of STT-MRAMs. For example, Everspin Technology announced the first STT-MRAM chip of 64Mb in 2012 [9] and the industry's first 1Gb pMTJ-based STT-MRAM in 2016 [10]. Intel and Samsung also demonstrated their embedded STT-MRAMs in 2018 [11,12].

Despite the bright prospect of STT-MRAM technology, an effective yet cost-efficient test solution is required before the mass production of STT-MRAM chips. Manufacturing tests are responsible for weeding out all *defective* chips prior to

shipment to end customers. Therefore, this is a very critical step in the entire VLSI design and manufacturing chain, since assembling a defective chip onto a board or a system causes enormous cost and may even damage the manufacturer's reputation. STT-MRAM manufacturing process involves not only standard CMOS processing steps, but also the fabrication and integration of MTJ devices which are the data-storing elements. The latter is subject to new manufacturing defects which have not been fully investigated so far. Furthermore, due to the adoption of new materials and novel physical phenomena, new failure mechanisms such as magnetic coupling, STT switching stochasticity, and thermal fluctuation may cause transient faults, leading to yield loss [13]. This shift in failure mechanisms may impact the fault modeling methodology and results. Note that accurate fault models which reflect the physical defects are crucial to develop a high defect coverage test solution, e.g., *defective part per billion* DPPB level. Therefore, to develop a good-quality test, attention needs to be paid to the following three aspects: 1) understanding all failure mechanisms in STT-MRAMs so as to have accurate simulation models for them; 2) accurate fault analysis and modeling; 3) test/design-for-testability (DfT) development to cover all faults.

This paper serves as a review of the-state-of-the-art on STT-MRAM testing. As this is still an emerging and ongoing research topic, we try to cover as much important related work as possible in the literature. We organize and discuss the contents at three abstraction levels, which are failure mechanisms, faults models, and tests. First, we categorize all failure mechanisms for STT-MRAMs into five categories: 1) manufacturing defects; 2) extreme process variations; 3) magnetic coupling; 4) STT-switching stochasticity; 5) thermal fluctuation. Each of them will be introduced in details. Second, fault models due to those failure mechanisms are also classified and discussed in depth. The first two failure

mechanisms result in permanent faults which are typically the targets of manufacturing tests. The other three, however, lead to transient faults which intermittently appear with certain occurrence rate in some specific cycles at run time. Thus, transient faults can be tolerated by circuit-level techniques or error correction codes (ECCs), and they should be excluded somehow in any tests to avoid yield loss. Third, test algorithms and DfT designs proposed in the literature are also covered in this paper. However, test solutions for STT-MRAMs are still far away from established yet. To obtain a high-quality test, more research work needs to be done on this topic at failure-mechanism, fault-model, and test levels.

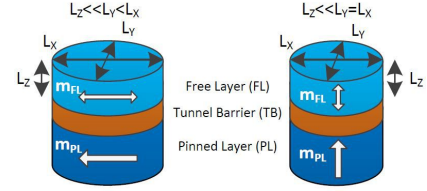
The rest of this paper is organized as follows. Our discussion begins with an introduction to MRAM technologies with an emphasis on STT-MRAM in Section II. Section III elaborates all failure mechanisms in STT-MRAM. Thereafter, we present fault models in Section IV. Section V and VI discuss test algorithms and DfT designs, respectively. The remaining challenges in STT-MRAM testing are presented in Section VII. Finally, we conclude this paper in Section VIII.

## II. MRAM BASICS

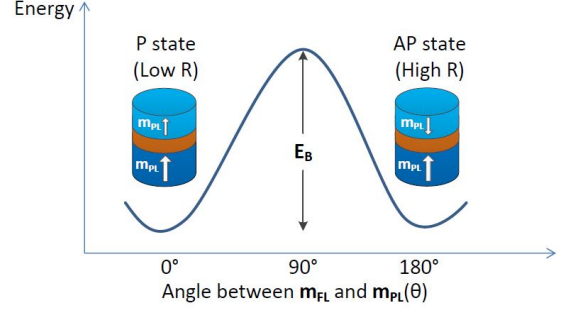
### A. MTJ Fundamentals

The *magnetic tunnel junction* (MTJ) is the most basic building block for MRAMs; it essentially consists of two ferromagnetic layers sandwiching an extremely thin insulating spacer layer, as illustrated in Fig. 1(a). The top ferromagnetic layer is called *free layer* (FL) which stores the binary information. This layer is usually made of CoFeB material. The magnetization of the FL points along its intrinsic easy axis and may flip by applying a spin-polarized current through it. The MTJ device can be *in-plane magnetic anisotropy* (IMA) [14–16] if the easy axis points along x-axis (the left one in Fig. 1(a)), or *perpendicular magnetic anisotropy* (PMA) [17–20] if along z-axis (the right one in Fig. 1(a)). The bottom ferromagnetic layer, referred to as *pinned layer* (PL) or *reference layer*, is used to provide a stable reference direction to the magnetization in the FL. Although made of CoFeB as well, its anisotropy energy is large enough to avoid switching during operations. The spacer layer in the middle is called *tunnel barrier* (TB), which serves as an insulating non-magnetic spacer between the FL and PL. In case the TB layer is very thin (typically  $\sim 1$  ns), quantum mechanical tunneling of electrons through the barrier makes the MTJ behave as a tunneling resistor, whose resistance depends exponentially on the barrier thickness. To evaluate the resistivity of MTJ devices, the *resistance-area* ( $RA$ ) product is commonly used in the MRAM community, as it is independent of the device size. Together, the above three layers form the fundamental structure of the MTJ device.

The resistance of the MTJ device is low when the magnetization directions in FL and PL are parallel (P) and high when anti-parallel (AP), as shown in Fig. 1(b). These two binary magnetic states enable the MTJ device to store one-bit data. The resistance difference between the P and AP states is attributed to the *tunneling magneto-resistance* (TMR) effect [21–23]. The TMR effect can be simply interpreted by the



(a) Simplified MTJ structures with IMA (left) and PMA (right).



(b) Energy barrier ( $E_B$ ) between P and AP states.

Fig. 1. Schematics of two basic MTJ structures and binary resistive states.

band model [23] where the good band matching in the P state leads to large tunneling conductance (i.e., low resistance), while the poor band matching in the AP state results in less electrons tunneling through the barrier (i.e., high resistance). To qualitatively evaluate the TMR effect, the *TMR* ratio is widely adopted. It is defined by

$$TMR = \frac{R_{AP} - R_P}{R_P} \times 100\%, \quad (1)$$

where  $R_{AP}$  and  $R_P$  are the resistances in AP and P states, respectively. The higher the *TMR*, the easier it becomes for sense amplifiers to distinguish the two magnetic states correctly (i.e., better readability). For commercially-feasible STT-MRAM products, a minimum *TMR* ratio of 150% is required [24].

In order to switch between the AP and P states, a sufficient programming current is required to overcome the energy barrier ( $E_B$ ) between the two states, as shown in Fig. 1(b).  $E_B$  is given by [6]:

$$E_B = K_{u2}V = \frac{\mu_0 M_s V H_k}{2}, \quad (2)$$

where  $K_{u2}$  is the second-order uniaxial anisotropy constant,  $V$  is the FL volume,  $M_s$  is the saturation magnetization, and  $H_k$  the magnetic anisotropy field. The energy barrier is key to the MTJ's *thermal stability* ( $\Delta$ ), which determines the retention time ( $t_{ret}$ ). The  $\Delta$  and  $t_{ret}$  are expressed as [23]:

$$\Delta = \frac{E_B}{k_B T}, \quad (3)$$

$$t_{ret} = t_0 \exp(\Delta), \quad (4)$$

where  $k_B$  is Boltzmann constant, and  $T$  is the temperature.  $t_0$  is the inverse attempt frequency ( $\sim 1$  ns). The higher the  $\Delta$ , the more stable the magnetic state of the MTJ and thus the more energy required to program it. For a nano-magnet with  $\Delta = 40$ , the retention time is around 7.4 years [25]. Typically,

$\Delta > 80$  is needed to meet the industrial requirement, i.e., a retention time larger than 10 years.

There are fundamentally two kinds of MTJ devices that have been widely investigated. The first generation of MTJ devices is based on IMA, as illustrated with the left diagram in Fig. 1(a). Despite many early attempts of MRAM demonstration chips [26] or even commercial toggle-MRAM products by Freescale/Everspin in 2006 [27], IMA-MTJs have many shortcomings, including: 1) the elliptical cross-section with an aspect ratio of 2-3 makes them vulnerable to process variation, 2) decreased thermal stability with shrinking dimension, 3) further slash on the switching current is impractical at advanced technology nodes. As a result, the above limitations of IMA-MTJs have shifted research interest to MTJ structures based on PMA. In PMA-MTJs, the uniaxial easy axis is perpendicular to the horizontal cross-section of MTJ (see the right side of Fig. 1(a)). PMA-MTJs offer many benefits over IMA-MTJs, e.g., its circular structure ( $L_Y = L_X$ ) makes it easier to scale to advanced nodes. Although there still exist many design challenges for PMA-MTJs, they are believed to be superior to the IMA-MTJs as building elements of STT-MRAMs at future technology nodes [28]. Therefore, we limit our focus on STT-MRAMs based on PMA-MTJs in the remainder of this paper.

## B. MRAM Classification

In the past two decades, various MRAM technologies have been introduced. Despite their differences, a key distinction between them is the switching method of the MTJ magnetic state. Based on this, MRAM technologies can be classified into three categories: magnetic-field switching MRAM, STT switching MRAM, and novel-mechanism switching MRAM. Each of them is explained next.

### 1) Magnetic-Field Switching MRAM

The first MRAM generation is magnetic-field switching MRAM (MF-MRAM). The MF-MRAM uses an external magnetic field to switch the magnetic state [29,30]. Typically, a write operation to an MF-MRAM cell is implemented by injecting current to metal lines above and below the addressed MTJ device. These current-carrying lines then generate magnetic fields to reverse the magnetization in FL. The biggest problem for MF-MRAM is half-selection. It means that all non-targeted bit-cells along the two metal lines are exposed to the programming magnetic field (i.e., half-selected). This may cause inadvertent bit flips.

The half-selection problem can be mitigated by the Savtchenko switching technique [31]. This technique reduces the sensitivity of the half-selected cells by adopting: 1) synthetic antiferromagnet (SAF) structure for FL; 2) fixed sequence of write current pulse to toggle between AP and P states for the MTJ devices. MF-MRAM based on the Savtchenko switching technique is also called toggle MRAM [32].

Despite several prototypes and even small-scale commercial products [27,33], many limitations make mass production infeasible. For example, one of the challenges of MF-MRAMs is technology downscaling. With technology shrinking, it is

increasingly difficult to maintain a low write disturb rate and high thermal stability [24]. Furthermore, the relatively high write current ( $\sim 10$  mA) [34] and complicated cell geometry [24] are also barriers to push MF-MRAMs to the market.

### 2) STT Switching MRAM

The spin-transfer-torque switching MRAM (STT-MRAM) [15,26,35,36] emerged as the second-generation of MRAM technology. It offers an alternative switching method that overcomes the scaling problems in MF-MRAMs. Due to the fact that STT-MRAMs leverage spin-polarized current to reverse the magnetization direction in FL, they have a much simpler memory cell geometry, eliminating the landing pads, word and bypass lines required in MF-MRAMs. This makes it possible to scale the cell size of STT-MRAMs down to 4-6 F<sup>2</sup>, compared to 20-30 F<sup>2</sup> for MF-MRAMs. Therefore, research focus from both academia and industry has shifted from MF-MRAMs to STT-MRAMs for technology nodes of 90 nm and below [24].

The STT switching process can be modeled by the Landau-Lifshitz-Gilbert (LLG) equation, which describes the magnetization dynamics of FL [36–38]:

$$\begin{aligned} \frac{d\mathbf{m}_{\text{FL}}}{dt} &= \mathbf{\Gamma}_{\text{prec}} + \mathbf{\Gamma}_{\text{damp}} + \mathbf{\Gamma}_{\text{IP}}^{\text{STT}} + \mathbf{\Gamma}_{\text{P}}^{\text{STT}} \\ \mathbf{\Gamma}_{\text{prec}} &= -\gamma\mu_0\mathbf{m} \times \mathbf{H} \\ \mathbf{\Gamma}_{\text{damp}} &= -\alpha\gamma\mu_0\mathbf{m} \times (\mathbf{m} \times \mathbf{H}) \\ \mathbf{\Gamma}_{\text{IP}}^{\text{STT}} &= \gamma\mu_0\eta\frac{\hbar J}{2e} \frac{1}{M_s t} \mathbf{m}_{\text{FL}} \times (\mathbf{m}_{\text{FL}} \times \mathbf{m}_{\text{RL}}) \\ \mathbf{\Gamma}_{\text{P}}^{\text{STT}} &= \gamma\mu_0\eta'\frac{\hbar J}{2e} \frac{1}{M_s t} \mathbf{m}_{\text{FL}} \times \mathbf{m}_{\text{RL}}. \end{aligned} \quad (5)$$

In these equations,  $\mathbf{m}_{\text{FL}} = \frac{\mathbf{M}_{\text{FL}}}{M_s}$  is the normalized magnetization vector  $\mathbf{M}_{\text{FL}}$  in FL with respect to the saturation magnetization  $M_s$ ,  $\mathbf{H}$  the total effective magnetic field (including anisotropy and applied fields),  $\alpha$  the Gilbert damping,  $\gamma$  the gyromagnetic ratio, and  $\mu_0$  the vacuum permeability,  $J$  the current density,  $t$  the thickness of FL,  $e$  the electron charge, and  $\hbar$  the Planck constant. The term  $\mathbf{\Gamma}_{\text{prec}}$  in Equation (5) describes the precessional motion of the magnetization around the effective field  $\mathbf{H}$ , while the term  $\mathbf{\Gamma}_{\text{damp}}$  describes the gradual damping of the magnetization precessional motion toward the effective magnetic field  $\mathbf{H}$ . The term  $\mathbf{\Gamma}_{\text{IP}}^{\text{STT}}$  and  $\mathbf{\Gamma}_{\text{P}}^{\text{STT}}$  are the spin-polarized current induced torque acting on the  $\mathbf{m}_{\text{FL}}$ , leading to a flip to the opposite direction.

By solving the LLG equation, the following expression for the critical switching current density ( $J_{c0}$ ) of the PMA-MTJs is derived [37]:

$$J_{c0}^{\text{PMA}} = \frac{1}{\eta} \frac{2\alpha e}{\hbar} (M_s t) (H_k). \quad (6)$$

This parameter is intrinsically determined by the MTJ design itself (e.g., materials, dimensions, and structure). This makes it possible to compare the difficulty of switching the magnetic state (i.e., writability) among various MTJ designs. However, the actual switching process depends on both the amplitude and duration of the programming current in practical circuit designs [39]. The higher the programming current density ( $J_c$ ) with respect to the  $J_{c0}$ , the less the time required to complete

a switching process. According to the duration of programming current pulse, two regimes are commonly observed to account for the switching process [40–42]. For very short pulses ( $t_p < 10$  ns),  $J_c$  has to be much larger than the  $J_{c0}$  to successfully switch the magnetization in FL. This is commonly referred to as the precessional regime, where the magnetization reversal is caused by STT effects. For longer pulses ( $t_p > 50$  ns), it is still possible that the magnetization in FL flips even if  $J_c < J_{c0}$ . This switching regime is called thermal activation regime, where the thermal fluctuation dominantly results in a magnetization flip. In practice, the programming current lies in the precessional regime to reduce the write latency, while guaranteeing a determinative flip. Switching events in the thermal activation regime are one of the causes of undesired transient faults in STT-MRAMs.

Although STT-MRAM is considered as one of the most promising NVM technologies for both embedded and stand-alone applications in the future, it suffers from a few weaknesses. For example, the read disturb is non-negligible at advanced nodes, since writing and reading operations share the same path through the two-terminal MTJ device. Another critical limitation is that the STT switching mechanism requires high currents ( $> 1$  MA/cm<sup>2</sup>) with pulse widths in the ns range [43]. These programming currents may result in both hard and soft breakdown of the ultra-thin MgO barrier [44–47].

### 3) Novel-Mechanism Switching MRAM

Sveral new switching schemes are under investigation as the third-generation MRAM, including spin hall effect (SHE), spin-orbit torque (SOT), voltage-control-magnetic anisotropy (VCMA), etc. The research motivation behind these novel MRAM technologies is that the switching energy can be further reduced, while boosting writing performance. The SHE effect utilizes spin current generated in the direction transverse to the charge current to switch the magnetization, which can be one order of magnitude less than the switching current in STT-MRAMs [48]. Since the effective spin injection efficiency can reach as high as 100%, the SHE writing mechanism has the potential to be faster ( $> 1$  GHz) and more energy efficient ( $< 0.1$  pJ/bit) [49]. Recently, the SOT switching mechanism has been introduced to MRAM. It offers an ultra-fast writing capacity with a higher reliability compared to the STT solution [50,51]. Furthermore, The three-terminal setup of SOT-MTJ devices has separate read and write current paths, thereby solving the read disturb problem in STT-MRAM. The VCMA-MRAM is an another promising alternative to STT-MRAMs for low energy consumption applications [52]. It has the potential to simultaneously achieve ultrahigh storage density, ultralow energy consumption, and GHz high-speed operation at room temperature [53]. However, the uncontrollable random write-errors pose a severe reliability problem that needs to be overcome, since the VCMA only lowers the energy barrier between two magnetization polarizations.

In summary, three generations of MRAM technologies are under development based on the switching mechanism of MTJ magnetic state. The first-generation MF-MRAM faces a number of challenges, especially the advanced scaling impeding its way to commercialization. The third-generation MRAM

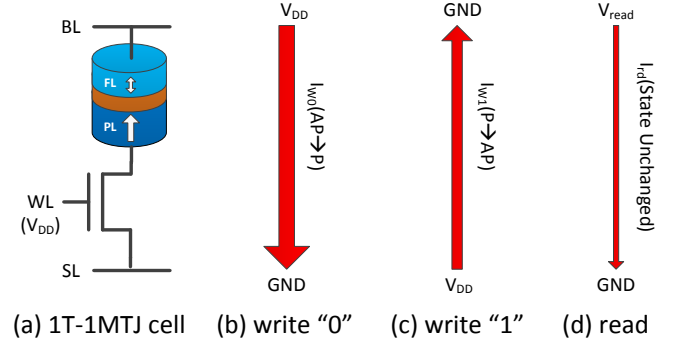


Fig. 2. Write and read operations on a 1T-1MTJ cell.

technologies are still in infancy stage and require further innovations in materials, reliability enhancement, manufacturing feasibility, etc. In contrast, STT-MRAM is currently the closest to wide deployment for a number of applications, such as consumer and industrial controllers, data centers, internet of things, and automotive [54]. We will limit our discussion to STT-MRAM in the remainder of this paper.

### C. 1T-1MTJ Bit-cell Design

The 1T-1MTJ bit-cell design is the most widely-adopted cell design, comprising an MTJ device connected serially with an access transistor [55,56], as shown in Fig. 2(a). The MTJ in this structure serves as a resistive storage element, while the access transistor, typically NMOS, is responsible for selective access. The NMOS gate is connected to a word line (WL), which determines whether a row is accessed or not. The other two terminals are connected to bit line (BL) and source line (SL), respectively. They control write and read operations on the internal MTJ device depending on the magnitude and polarization of voltage applied across them.

Fig. 2(b)–(d) show the three basic operations: write “0”, write “1”, and read. During a write “0” operation, WL and BL are pulled up to  $V_{DD}$  and SL is grounded, thus leading to a current ( $I_{w0}$ ) flowing from BL to SL. In contrast, a write “1” operation requires the opposite current through the MTJ device with WL and SL at  $V_{DD}$ , and BL grounded. In order to avoid write failures, write currents in both directions should be greater than the critical switching current  $I_c$ . However, the current during a write “1” operation ( $I_{w1}$ ) is slightly smaller than during a write “0” operation ( $I_{w0}$ ), due to the source degeneration of NMOS in write “1” operations [57,58]. For read operations, a read voltage  $V_{read}$  is applied; it leads to a read current ( $I_{rd}$ ) with the same direction as  $I_{w0}$  to sense the resistive state (AP/P) of MTJ.

To avoid an inadvertent state change during read operations, known as *read disturb*,  $I_{rd}$  should be as small as possible; typically  $I_{rd} < 0.5I_c$  for MTJs with a thermal stability of  $\Delta = 60$  [59]. However, a too low  $I_{rd}$  may lead to *incorrect read fault* [60]. In general, the current magnitude relations must satisfy:  $I_{rd} < I_c < I_{w1} < I_{w0}$ . This is indicated by the widths of the red arrows in Fig. 2. A read operation requires a sense



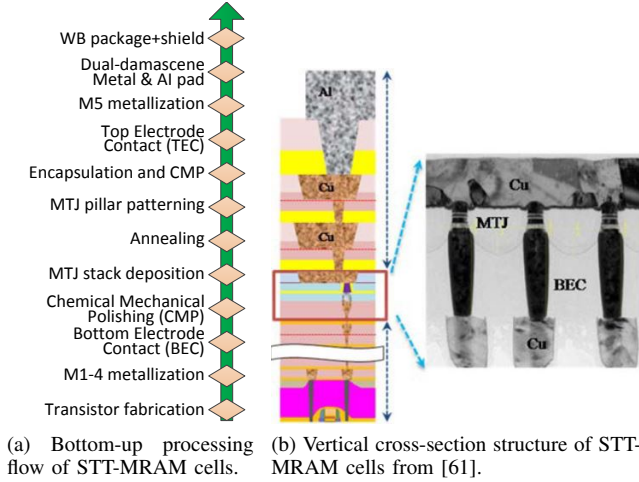


Fig. 3. General manufacturing process of STT-MRAM.

amplifier to determine the resistive state. The sense amplifier may be implemented using a current sensing scheme, where the read-out value is determined by comparing the current of the accessed cell ( $I_{\text{cell}} = I_{\text{rd}}$ ) with the current of a reference cell ( $I_{\text{ref}}$ ). The sensing result is logical “0” if  $I_{\text{cell}} < I_{\text{ref}}$ ; otherwise, it outputs logical “1”.

### III. FAILURE MECHANISMS

Despite the small-scale manufacturability of STT-MRAM demonstrated by several semiconductor companies including Intel and Samsung, STT-MRAM-specific failure mechanisms need to be fully studied and addressed before mass production. First, the fabrication of STT-MRAM chips requires a more sophisticated manufacturing process, including not only the mature CMOS fabrication steps, but also the MTJ fabrication and integration. The latter may also introduce new defects, which unfortunately have not been fully investigated to date. Second, the exploitation of magnetic materials and novel physical phenomena makes STT-MRAMs suffer from some unique failure mechanisms including magnetic coupling, STT stochastic switching, and thermal fluctuation. In this section, we first discuss all potential manufacturing defects in STT-MRAMs. Thereafter, we introduce the three STT-MRAM-specific failure mechanisms.

#### A. Manufacturing Defects

A defect is a physical imperfection in the processed wafer (i.e., an unintended difference from the intended design) [62]. To guarantee a high-quality test solution as well as to improve the manufacturing process itself so as to improve yield, understanding all potential defects is of great importance. The STT-MRAM manufacturing process mainly consists of the standard CMOS fabrication steps and the integration of MTJ devices into metal layers (e.g., between M4 and M5 layers [63,64]). Fig. 3(a) shows the bottom-up processing flow and Fig. 3(b) the vertical cross-section structure of STT-MRAM cells. Based on the manufacturing phase, STT-MRAM defects can be classified into front-end-of-line (FEOL) and back-end-of-line (BEOL) defects. As MTJs are integrated into metal

| TABLE I<br>STT-MRAM DEFECT CLASSIFICATION.  |   |  |
|---|---|--|
| FEOL  | BEOL  |  |
| Transistor fabrication  | MTJ fabrication   | Metalization   |
| Material impurity<br>Crystal imperfection<br>Pinholes in gate oxides<br>Shifting of dopants | Pinholes in MgO barrier<br>Extreme thickness variation of TB<br>MgO/CoFeB interface roughness<br>Atom inter-diffusion<br>Redepositions on MTJ sidewalls<br>Magnetic layer corrosion | Open vias/contacts<br>Irregular shapes<br>Big bubbles<br>Small particles |



Fig. 4. An open contact defect between the BEC and the underlying Cu layer. Reprinted from [61].

layers during BEOL processing, BEOL defects can be further categorized into MTJ fabrication defects and metalization defects. All potential defects are listed in Table I. Next, we will examine them in detail along with their corresponding processing steps, with a particular emphasis on those introduced during MTJ fabrication.

#### 1) FEOL Defects

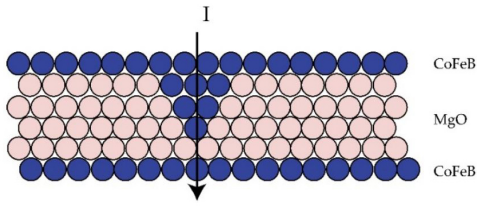
The first step of the STT-MRAM manufacturing process is the FEOL process where transistors are fabricated on the wafer. In this phase, typical defects may occur such as semiconductor impurities, crystal imperfections, pinholes in gate oxides, and shifting of dopants [66,67]. These are the conventional defects which have been sufficiently studied and are generally modeled by resistive opens, shorts and bridges [68–70].

#### 2) BEOL Defects

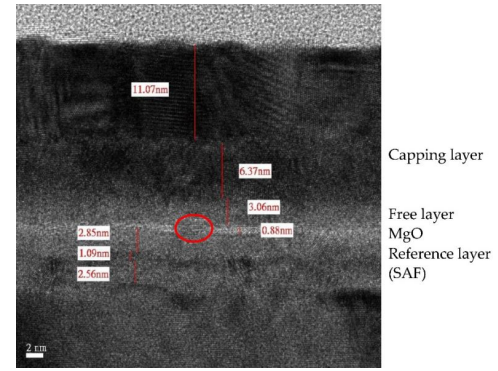
After FEOL, M1-M4 metal layers are stacked on top of the transistors followed by a bottom electrode contact (BEC), as illustrated in the zoomed-in part of Fig. 3(b). M1-M4 metalization does not differ from traditional CMOS BEOL steps. The BEC step is used to connect bottom Cu lines with MTJ stacks [61,71]. During this phase, typical interconnect defects may take place, such as open vias/contacts, irregular shapes, big bubbles, etc. [68]. Song et al. [61] provided a transmission electron microscopy (TEM) image of an open contact, as shown in Fig. 4. The open contact between the underlying Cu line and BEC is caused by polymer leftovers.

To obtain a super-smooth interface between the BEC and the MTJ stack, a chemical mechanical polishing (CMP) step is required. The smoothness of the interface between layers is key to obtaining a good *TMR* value. CMP processing minimizes the surface roughness with a root-mean-square (RMS) average of 2 Å [63]. At this stage, both under-polishing and over-polishing of the surface can introduce defects. Specifically, under-polishing causes issues such as orange peel coupling or offset fields which affect the hysteresis curve, while over-polishing may result in dishing or residual slurry particles that are left behind [72].

After the CMP step, the next critical step is to fabricate the



(a) Schematic of a MTJ stack with a pinhole in the MgO tunnel barrier.



(b) Cross-section TEM of a MTJ with a pinhole defect.

Fig. 5. Pinhole defect in the tunnel barrier of an MTJ device. Reprinted from [65]

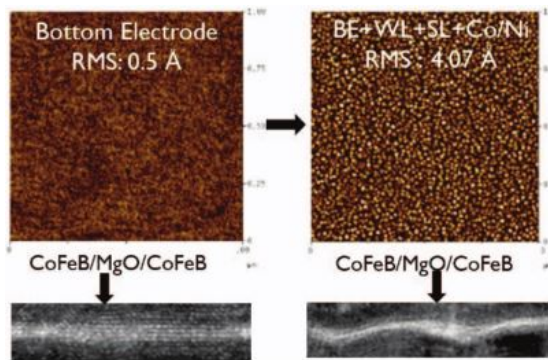


Fig. 6. The MgO/CoFeB interface is rougher for an advanced MTJ stack design (right) with an iSAF pinned layer than a simple MTJ stack design (left). Reprinted from [71].

MTJ stack. The latest published MTJ stack design consists of more than 10 films including a complicated inner synthetic anti-ferromagnetic (iSAF) pinned layer for performance reason [73]. However, the increasingly sophisticated MTJ design also makes it more vulnerable to manufacturing defects. For example, pinholes in the tunnel barrier (e.g., MgO) could be introduced in this phase. Fig. 5(a) illustrates the concept of a pinhole defect, and Fig. 5(b) shows a vertical cross-section TEM image of a deposited MTJ stack with a pinhole in its 0.88 nm tunnel barrier [65]. In this defective MTJ device, a pinhole forms in the tunnel barrier due to the rough deposition of MgO. As the CoFeB free layer is deposited on top of the tunnel barrier, the pinhole is filled with CoFeB material, as indicated by the red circle in Fig. 5(b). Therefore, the pinhole filled with CoFeB material forms a defective high-conductance path across the two ferromagnetic layers. It severely degrades the resistance and TMR value, and may even lead to breakdown due to the ohmic heating when an electric current passes through the barrier [74]. Furthermore, the MgO barrier thickness variation and interface roughness result in degradation of resistance and TMR values as well. TEM images in [65] show that the MgO barrier thickness varies from 0.86 nm to 1.07 nm, leading to a huge difference in resistance. Fig. 6 shows with images of atomic force microscopy (top two) and high-resolution transmission electron

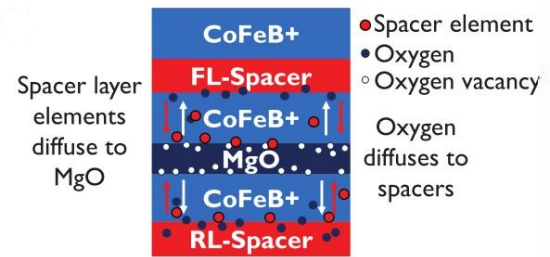
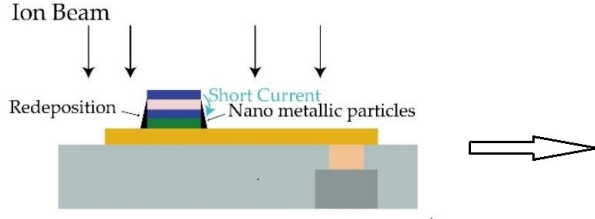


Fig. 7. Schematic of atom inter-diffusion mechanism showing that oxygens diffuse out of the MgO barrier into neighboring layers while spacer layer materials diffuse into the MgO layer. Reprinted from [43].

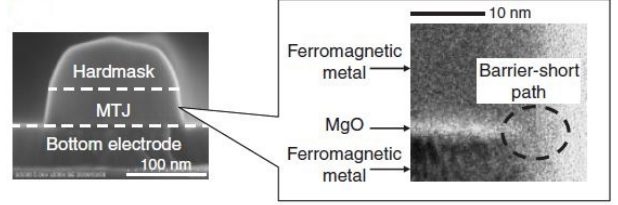
microscopy (bottom two) that a complicated iSAF pinned layer design elevates interface roughness from 0.5 Å to 4.07 Å. The increased interface roughness leads to significant TMR degradation [71].

After the MTJ stack deposition, annealing is applied to obtain crystallization in MgO barrier as well as in CoFeB PL and FL layers [76,77]. At this stage, the PMA originating from the MgO/CoFeB interface and TMR value are strongly determined by the annealing conditions such as temperature, magnetic field and annealing time. With appropriate annealing conditions, the PMA can be considerably enhanced, leading to higher thermal stability. Under-annealing can lead to lattice mismatch between the body-centered cubic (bcc) CoFeB lattice and the fcc MgO lattice, whereas over-annealing introduces atom inter-diffusion between layers. As illustrated in Fig. 7, oxygen atoms can diffuse out of MgO, leaving behind oxygen vacancies, thus severely degrading TMR value [43]. Worse still, diffusion of Ta from the seed layer to MgO layer has been reported in several papers [78,79], which scavenges O from MgO.

After MTJ multi-layer deposition, annealing and optical lithography processing, the next crucial step is to pattern individual MTJ nanopillars [80]. Typically, Ion beam etching (IBE) is widely used to pattern MTJ nanopillars [75,81]. Fig. 8(a) illustrates the etching process, where Ar ion beams are ionized and accelerated in a chamber and subsequently irradiate the wafer underneath, leading to selective etching of the area where a hard mask does not cover. During the MTJ



(a) Schematic of ion beam etching with redeposition on the MTJ sidewall. Reprinted from [65].



(b) Vertical cross-section TEM images of an MTJ device with sidewall redeposition. Reprinted from [75].

Fig. 8. Magnetic material redeposition defect on the sidewall of MTJ devices.

etching process, it is extremely difficult to obtain desired MTJ nanopillars with steep sidewall edges, while avoiding sidewall redeposition and magnetic layer corrosion. The redeposition phenomenon on MTJ sidewall may significantly deteriorate the electrical property of the MTJ device, and even cause a barrier-short defect shown in Fig. 8(b). In order to mitigate the redeposition effect, a side-etching step combined with the Halogen-based reactive ion etching (RIE) and inductively-coupled plasma (ICP) techniques [82–84] is needed by rotating and tilting the wafer. Nevertheless, other concerns arise. For instance, the shadowing effect (limited etching coverage at the lower corner of the MTJ profile due to insufficient spacing between MTJs) [65,75] limits a high-density array patterning, and magnetic layer corrosion degrades the reliability of MTJ devices due to the non-volatile chemicals attached to the CoFeB layers.

After MTJ etching processing, encapsulation and CMP are required to separate individual MTJ pillars. In this step, an oxygen showering post-treatment (OSP) can be applied to recover patterning damage so as to improve the electric and magnetic properties of MTJ devices [85]. The oxygen showering process selectively oxidizes the perimeter (damaged by previous ion beam etching) of the MTJ pillar with non-reactive oxygen ions. However, over-oxidization too much into the MTJ device also causes degradation in key device parameters such as TMR. Thus, the OSP condition needs to be carefully tuned to maximize the damage suppression while protecting the inner undamaged parts.

Next, MTJ pillars are connected to top electrode contact (TEC), followed by M5 metallization. The rest of manufacturing process are same as the BEOL steps of CMOS technology. Typical defects such open contact/vias, small particles etc. can occur in this phase as well. It is worth-noting that a package-level magnetic shield can be added to enhance the stand-by magnetic immunity of STT-MRAMs, as proposed in [86]. The magnetic shield was reported to be effective in protecting STT-MRAMs against external magnetic fields.

### B. Extreme Process Variations

Apart from manufacturing defects and magnetic coupling induced defects that we discussed in the previous section, extreme process variations are another probable cause of permanent faults in STT-MRAMs [87,88]. Process variations can be introduced at each step of the STT-MRAM manufacturing

process, leading to parasitic variations in both MTJs and transistors. Some key MTJ parameters affected significantly by process variations are listed as follows [88,89]:

- Magnetic anisotropy ( $H_k$ )
- Saturation magnetization ( $M_s$ )
- Tunnel magnetoresistance ratio (TMR)
- Tunnel barrier thickness ( $t_{ox}$ )
- Cross-sectional area ( $A$ )

Similarly, the fabrication of transistors also introduces cell-to-cell variations in some key parameters, such as the threshold voltage ( $V_{th}$ ) and the transistor size ( $L \times W$ ), caused by random dopant fluctuations and line-edge roughness, etc. [90,91]. As CMOS transistors not only reside in memory cells (serving as access controllers) but also in peripheral circuits, process variations of transistors also have a detrimental impact on STT-MRAMs. Process variations in the access NMOSs of bit-cells mainly affect their current driving capabilities during write/read operations, whereas process variations of transistors in peripheral circuits result in reliability degradation of write and read operations (e.g., sensing margin decrease).

All these parametric variations in both MTJs and transistors pose a huge threat to STT-MRAM designs. In practice, the worst case has to be considered and enough guard bands must be provided in designs for a target failure probability, typically  $\sim 10^{-9}$  for a  $6\sigma$  corner [88]. However, the band-guard scheme also results in serious performance sacrifice. The authors in [88] claimed that the  $6\sigma$ -corner values of write latency are 3.5x larger than the mean value for a given thermal stability  $\Delta = 60$ . Furthermore, this guard-band scheme has been afflicted by another notorious drawback, which is energy waste for the majority of cells in an STT-MRAM array. Under the circumstance of mass production, those cells with around or over  $6\sigma$  parameter deviation are inevitable to suffer from permanent faults as follows.

### C. Magnetic Coupling

As STT-MRAMs store data as relative orientation of magnetizations in the FL and PL of MTJ devices, the stability of magnetic states in these two ferromagnetic layers is vulnerable to any extra unintended magnetic fields externally or internally. As introduced in Section II-A, an MTJ device is composed of multiple ferromagnetic layers, which all inevitably generate *stray fields* ( $H_{stray}$ ) in the space [92]. These stray fields in turn have an impact on the stability of magnetization in the FL



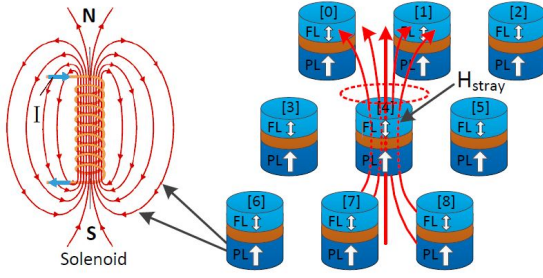


Fig. 9. Schematic of magnetic coupling. Neighboring cells 0-3 and 5-8 (aggressors) together generate an unintended stray field  $H_{\text{stray}}$  at the central cell 4 (victim).  $H_{\text{stray}}$  always exists during the lifetime of STT-MRAMs with its magnitude varying with the data pattern in the neighborhood.

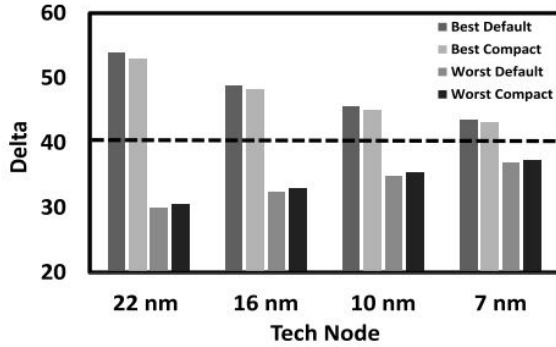


Fig. 10.  $\Delta$  variation (nominal  $\Delta = 40$ ) due to magnetic coupling with respect to various technology nodes for PMA-MTJs. The spacing in the default cell array is 5F, whereas it is 3F in the compact array. Reprinted from [97].

[93–96].  $H_{\text{stray}}$  varies with the MTJ ferromagnetic materials, stack design, dimensions, spacing, and process variation from device to device. Apart from the intra-cell stray fields, the ferromagnetic layers from neighboring cells also generate stray fields [97]. Therefore, all these intra-cell and inter-cell stray fields together can form a net offset field ( $H_{\text{offset}}$ ) on the FL of a specific MTJ within an STT-MRAM array. The effect of  $H_{\text{offset}}$  on a victim cell is usually referred to as *magnetic coupling*. As technology scales down, STT-MRAM cells move even closer to each other; this further aggravates the magnetic coupling problem. Thus, it is of great importance to investigate the effect of magnetic coupling on the STT-MRAM performance and reliability.

Fig. 9 shows a  $3 \times 3$  PMA-MTJ array. All ferromagnetic layers (i.e., FLs and PLs) of MTJs in the neighborhood of MTJ 4 together generate a net offset field  $H_{\text{offset}}$  acting on the victim MTJ 4 in the center. The stray field of a single ferromagnetic layer can be modeled as the magnetic field of a solenoid, shown in Fig. 9. The amount of current for the solenoid to generate the same amount of magnetization in any ferromagnetic layer can be calculated by  $\frac{M_s t}{N}$  [97], where  $M_s$  is the saturation magnetization,  $t$  is the thickness of the ferromagnetic layer, and  $N$  is the number of coils. By means of this solenoid model, we can approximately calculate  $H_{\text{stray}}$  of each ferromagnetic layer at any spot in space by the Biot-Savart law. Therefore,  $H_{\text{offset}}$  at the FL point in the victim MTJ 4 can be derived for a given data pattern in the  $3 \times 3$  MTJ array.

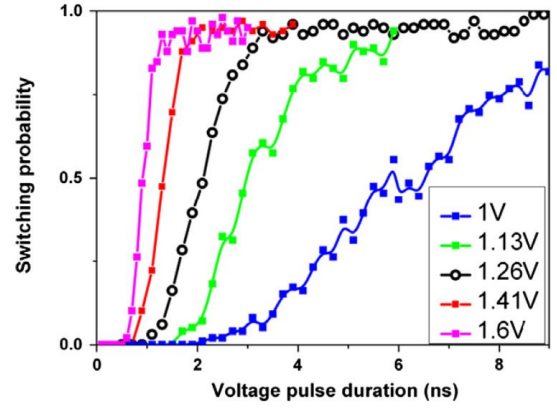


Fig. 11. Experimental measurements of STT-induced switching probability vs. duration and amplitude of the applied voltage pulse. Reprinted from [98].

The magnetic coupling effect has an impact on various MTJ parameters. Firstly, the thermal stability  $\Delta$  of the MTJ may deviate from its nominal value either positively or negatively depending on the direction of  $H_{\text{offset}}$  with respect to the anisotropy field  $H_k$  of the MTJ's FL. The effect of  $H_{\text{offset}}$  on  $\Delta$  can be described by [23]

$$\Delta(H_{\text{offset}}) = \Delta(H_{\text{offset}} = 0) \left(1 \pm \frac{H_{\text{offset}}}{H_k}\right)^2. \quad (7)$$

For example,  $H_{\text{offset}}$  reaches its peak when the data pattern is  $[111x, 1111]$ , indicating that all the neighboring MTJs are in AP state [97]. In this case, the thermal stability  $\Delta$  of the central victim MTJ 4 is enhanced to the best extent if it is in P state (i.e.,  $x = 0$ ). Conversely, the worst data pattern  $[1111, 1111]$  weakens the  $\Delta$  value to its rock bottom. Fig. 10 shows the  $\Delta$  values under the best data pattern and the worst data pattern with regard to various technology nodes. The gap between the best and worst cases is slightly over 50% of the nominal  $\Delta = 40$  at 22 nm node, and it shrinks with technology scaling down. This is because  $H_k$  increases faster than  $H_{\text{offset}}$  in order to maintain the nominal  $\Delta$  at 40 for various technology nodes [97].

Secondly, the magnetic coupling effect also influences the critical switching current density  $J_{c0}$ . The effect of magnetic coupling on  $J_{c0}$  can be characterized by adding a  $H_{\text{offset}}$  term to Equation (6) [23]:

$$J_{c0}^{\text{PMA}} = \frac{1}{\eta} \frac{2\alpha e \mu_0}{\hbar} (t M_s H_k) \left(1 \pm \frac{H_{\text{offset}}}{H_k}\right). \quad (8)$$

As an MTJ device with a higher  $\Delta$  requires a larger write current to switch the magnetization in the FL, the best data pattern for  $\Delta$  now becomes the worst case for  $J_{c0}$ . Similarly, the worst data pattern for  $\Delta$  becomes the best case for  $J_{c0}$ , meaning that a smaller write current is required to reverse the magnetization in the FL. Consequently,  $J_{c0}$  variation due to magnetic coupling amplifies the stochasticity of the STT switching behavior, thus necessitating a large write margin to maintain an acceptable write error rate for all memory cells.

#### D. STT-switching Stochasticity

In Section II-B, we have briefly introduced the STT-induced switching mechanism. For a write current pulse shorter than



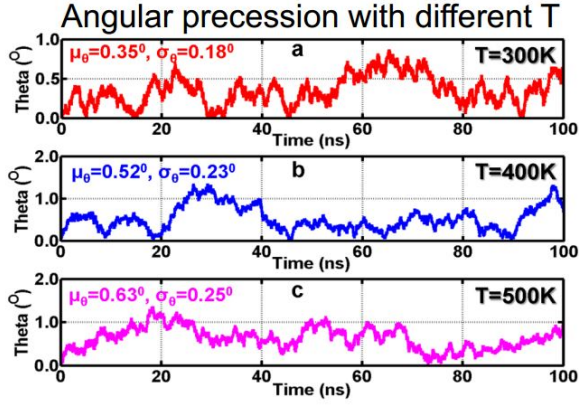


Fig. 12. Thermally-induced initial angle oscillation over time under the ambient temperature of 300K, 400K, and 500K. Reprinted from [101].

10 ns, the STT-effect dominantly results in a magnetization switching action if the density of the spin-polarized current flowing through the FL of MTJ device is larger than the critical switching current density ( $J_c > J_{c0}$ ). The LLG equation (5) models the magnetization dynamics of the precessional switching process. However, the actual switching time varies from one event to the next, due to the fact that the STT-switching is intrinsically stochastic [98]. According to the experiments and theoretical analysis in [99], after the write pulse onset there exists a ns-scale incubation delay time varying significantly for individual events. Then, it is followed by an abrupt precessional switching of the magnetization for around 400 ps. Therefore, a switching failure occurs when the incubation time gets longer than the fixed pulse width of write operations.

Fig. 11 shows the switching probability of the magnetization in the FL versus the amplitude and duration of the applied voltage pulse. It can be seen that the switching probability increases remarkably with the pulse duration and amplitude before reaching an saturation level close to 100%. Thus, increasing the write current amplitude or duration is an effective method to avoid write failure [98,100]. However, this approach also leads to significant power and speed overhead, which has posed a major obstacle to the potential application of STT-MRAMs as last level caches (LLCs).

#### E. Thermal Fluctuation

Thermal fluctuation has a great impact on the STT-switching behavior; it increases the cycle-to-cycle magnetization switching variation [103]. The effect of thermal fluctuation on the STT-switching behavior can be characterized by modifying the LLG Equation (5), taking into consideration the thermally-induced random field ( $H_{fluc}$ ) and the initial angle ( $\theta$ ) between the magnetizations in the FL and the PL [89,104,105]:

$$\begin{aligned} \frac{d\mathbf{m}_{FL}}{dt} &= \mathbf{\Gamma}_{prec} + \mathbf{\Gamma}_{damp} + \mathbf{J}(\theta)(\mathbf{m} \times \mathbf{m} \times \mathbf{m}_{RL}) \quad (9) \\ \mathbf{\Gamma}_{prec} &= -\gamma\mu_0\mathbf{m} \times (\mathbf{H} + \mathbf{H}_{fluc}) \\ \mathbf{\Gamma}_{damp} &= -\alpha\gamma\mu_0\mathbf{m} \times (\mathbf{m} \times (\mathbf{H} + \mathbf{H}_{fluc})), \end{aligned}$$

where  $\mathbf{J}(\theta)$  is the coefficient of the STT term, depending on the initial angle ( $\theta$ ) between the magnetizations in the FL and the PL. Based on the above equation, Wang et al. [103] claimed that thermal fluctuation not only influences the STT-switching time distribution, but also plays a major role in determining the magnetization reversal for a long pulse width (typically  $>100$  ns) in the thermal activation regime. In other words, a small current even lower than the critical switching current density ( $J_c < J_{c0}$ ) is still possible to reverse the magnetization in the FL. This situation may occur in read operations, thus causing a read disturb fault. Worse still, an unexpected magnetization flip may happen even if no current flows through the MTJ device, leading to a retention fault. For the thermally-induced switching under a long pulse, the switching probability can be estimated by the Neel-Brown model [106]

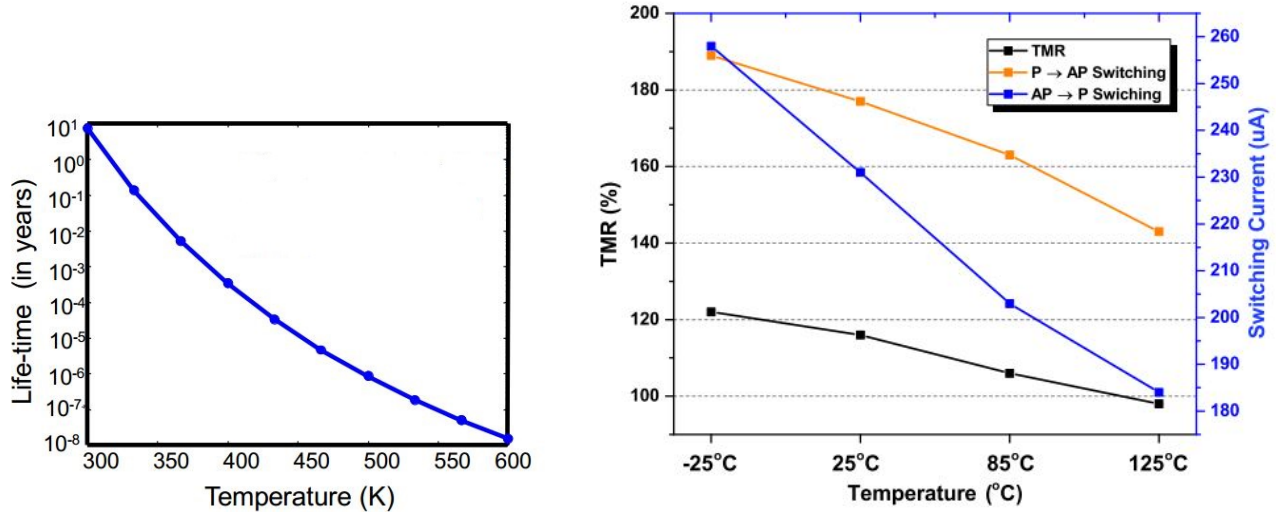
$$\begin{aligned} Pr(t) &= 1 - \exp(-t/\tau_1) \quad (10) \\ \tau_1 &= \tau_0 \exp(\Delta(1 - I/I_{c0})), \end{aligned}$$

where  $\tau_0$  is the attempt time ( $\sim 1$  ns) characterizing the timescale under which the magnetization can be considered practically at rest, and  $\tau_1$  represents the averaged switching time.  $I$  and  $t$  are the amplitude and duration of the applied current, respectively.  $I_{c0}$  is the critical switching current.

Furthermore, the thermal fluctuation magnitude significantly depends on the ambient temperature. The effect of temperature is twofold. First, thermal fluctuation agitates a random initial angle ( $\theta$ ) between the magnetizations in the FL and the PL, and both the mean value and the standard deviation  $\theta$  increase with temperature [23,107]. Fig. 12 shows that the oscillation intensity of  $\theta$  is nearly doubled as the temperature goes from 300K to 400K. This makes STT-MRAMs subject to severe reliability problems at elevated temperature. Second, temperature has a significant influence on some MTJ parameters, such as  $\Delta$ , TMR, and switching current. According to equation (2-4), since  $\Delta$  is inversely proportional to temperature, the lifetime of data stored in STT-MRAM cells decreases exponentially with temperature, as shown in Fig. 13(a). Zhao et al. found that  $R_{AP}$  decreases while  $R_P$  barely changes when the temperature rises [108–110]. As a result, TMR value goes down with temperature, as shown in Fig. 13(b). This makes read margin shrink at elevated temperature, which may lead to an incorrect read fault. Apart from  $\Delta$  and TMR, the switching current also decreases with temperature [111]. However, this is actually a benefit for write operations, meaning that a shorter or smaller write pulse is required at higher temperature. By utilizing this phenomenon, thermally-assisted MRAMs have been proposed to briefly heat up the MTJ device in write operations to facilitate the magnetization reversal [112,113].

#### IV. FAULT MODELS

In the last section, we have introduced all potential defects that may take place in STT-MRAMs. The occurrence rate of these defects mainly depends on the manufacturing technology and process. To detect those defective STT-MRAM chips, it is prohibitively expensive to physically and manually examine



(a) The temperature dependence of data lifetime in MTJ devices. Reprinted from [101].

(b) The temperature dependence of TMR value and switching current. Reprinted from [102].

Fig. 13. The ambient temperature has a evident impact on MTJ parameters: (a) thermal stability (manifested as the lifetime of the stored data in MTJ devices), (b) TMR value and switching current.

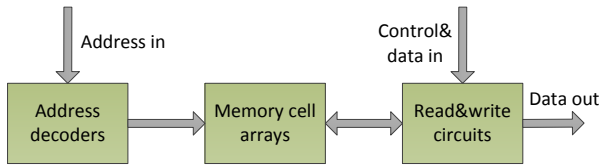


Fig. 14. Reduced functional memory model.

all manufactured chips. As an alternative, it is usually more efficient and cheaper to characterize and detect faulty behaviors from a functional perspective. This calls for accurate STT-MRAM fault models which are the representation of certain physical defects at the abstracted function level [62]. Despite the well-established fault models for traditional memory technologies, STT-MRAM, as an emerging NVM technology, may need unique fault models to cover all potential defects. In the section, we will present all proposed fault models in the literature.

#### A. Classifications

A memory chip can be functionally reduced to three blocks: address decoders, memory cell arrays, and read&write circuits, as shown in Fig. 14. Address decoders are concerned with addressing the right cell or word in a memory cell array. Memory cell arrays are composed of identical memory cells in a matrix form. Read&write circuits usually consist of sense amplifiers, pre-charge circuits, and write drivers; they are responsible for data transport from and to the addressed memory cell, respectively.

Fig. 15 illustrates the classification of memory faults based on three criteria: 1) location, 2) lifetime, and 3) physical nature. We will explain each of them as follows.

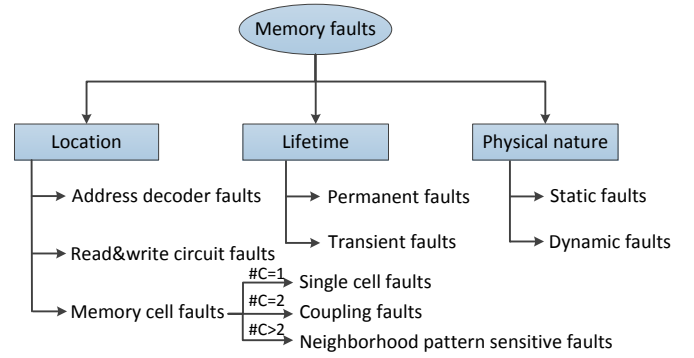


Fig. 15. Classification of memory faults.

##### 1) Location

According to the fault location, faults can be grouped into three categories: address decoder faults, memory cell array faults, and read&write circuit faults. Address decoder faults are concerned with those faults in the address decoders, such as *mismatch faults* between addresses and cells, *delay faults* due to the increased capacitance in word lines or bit lines, etc. Memory cell array faults refer to those faults taking place in memory cell arrays, such as *stuck-at-fault* (SAF), *transition fault* (TF), *coupling fault* (CF). Based on the number of involved cells, memory cell array faults can be further classified into: *single cell faults* ( $\#C=1$ ), *coupling faults* ( $\#C=2$ ), and *neighborhood pattern sensitive faults* ( $\#C>2$ ). Read&write circuit faults are those speed-related faults occurring in the read&write circuits, such as *slow sense amplifier fault* (SSAF) and *slow write driver fault* (SWDF). As memory cell arrays occupy the majority part of a memory chip, research efforts mainly focus on faults in this location while faults in the other

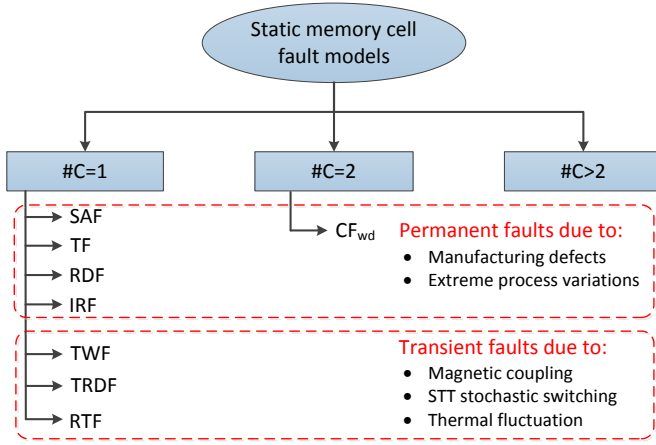


Fig. 16. Classification of static faults in STT-MRAM cell array.

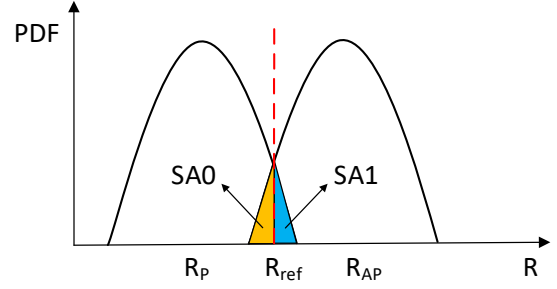
two locations are somewhat neglected. This is also the case for STT-MRAMs. All existing publications are dedicated to the analysis and detection of faults in memory cell arrays whereas faults in other locations have not been explored so far, to the best of our knowledge.

### 2) Lifetime

Based on the fault lifetime, faults can also be classified into two categories: permanent faults and transient faults [65,87,89]. The former refer to those faults that are permanent and uncorrectable, which can be caused by manufacturing defects and extreme process, voltage, or temperature (PVT) variations. Permanent faults feature cell-to-cell variation, which means that only a small fraction of memory cells are defective and thus do not function as expected, while the majority of cells function as well as intended in designs. Due to the deterministic effects of defects and PVT variations on memory cells after fabrication, permanent faults are generally fixed and detectable with certain testing techniques. The latter are those faults that are temporary, and they can be self-corrected by a new operation on the faulty cell. Instead of the cell-to-cell variation for permanent faults, transient faults introduce cycle-to-cycle variation. In other words, the fault occurrences are probabilistic and unpredictable during the lifetime of memory chips, due to the STT stochastic switching nature and thermal noise, etc. Therefore, transient faults should not be considered as the target during manufacturing tests [114]. However, it is worth noting that transient faults are increasingly becoming a reliability challenge, since PVT variations, thermal fluctuation, magnetic coupling, and radiation are no longer neglectable interference factors as technology scales down. Consequently, stronger ECCs or other correction techniques are required to correct these run-time faults.

### 3) Physical nature

Last but not least, faults can also be grouped into static faults and dynamic faults based on their physical natures. The former are generally not timing-related and require at most one operation ( $\#O \leq 1$ ) to be sensitized. The latter are often timing-related and require more than one consecutive operations ( $\#O > 1$ ) to be sensitized.

Fig. 17. Illustration of the SAF caused by resistance distribution tail overlap of  $R_P$  and  $R_{AP}$  due to extreme process variation in  $t_{ox}$  of the MTJ device.

## B. Static Faults in STT-MRAM Cell Arrays

In this part, we will mainly examine static faults occurring in STT-MRAM cell arrays, since research attempts to date are mainly of this category due to the dominant area of cell arrays in STT-MRAM chips. Fig. 16 shows the classification of all fault models that have been proposed in the literature in this category. Next, we will first introduce permanent fault models, including stuck-at-fault (SAF), transition fault (TF), read destructive fault (RDF), incorrect read fault (IRF), and write disturb coupling fault ( $CF_{wd}$ ). Thereafter, we will elaborate transient faults including transient write fault (TWF), transient read disturb fault (TRDF), and retention fault (RTF), which are mainly caused by STT-MRAM specific failure mechanisms such as STT stochastic switching nature and thermal perturbation.

### 1) Permanent Faults

**Stuck at fault (SAF):** this fault refers to that a cell always presents logical value 0 (SA0) or 1 (SA1), no matter what values are written into it. SA0 and SA1 faults are denoted as  $\langle \forall/0/- \rangle$  and  $\langle \forall/1/- \rangle$ , respectively. Similar to traditional charge-based RAMs, SAFs in STT-MRAMs can be caused by physical defects. For instance, the authors in [88] proposed that some resistive shorts or bridges (i.e., electrical equivalents to certain physical defects) in the STT-MRAM cell array can cause SAFs. Furthermore, process variations tend to deviate key MTJ and transistor parameters from their nominal values, leading to SAFs under extreme circumstances [87]. For example, the author in [65] observed that the MTJ tunnel barrier exhibits different thickness arranging from 0.86 nm to 1.07 nm, while the nominal value is 1 nm. As the MTJ resistance is exponentially dependent on the tunnel barrier thickness  $t_{ox}$ , a tiny  $t_{ox}$  variation will lead to a huge difference in resistance. Fig. 17 illustrates that the  $t_{ox}$  variation causes a partial overlap of  $R_P$  and  $R_{AP}$  distributions. An MTJ device with  $R_P$  falling in the tail over  $R_{ref}$  would suffer from a SAF1 fault, whereas the lower tail of  $R_{AP}$  distribution under  $R_{ref}$  would lead to a SA0 fault. As technology scales down, reducing process variation in  $t_{ox}$  becomes increasingly challenging during fabrication.

**Transition Fault (TF):** this fault refers to that a cell fails to make a rising transition ( $0 \rightarrow 1$ ) or a falling transition ( $1 \rightarrow 0$ ) when it is written. TF includes TF0 and TF1, which are



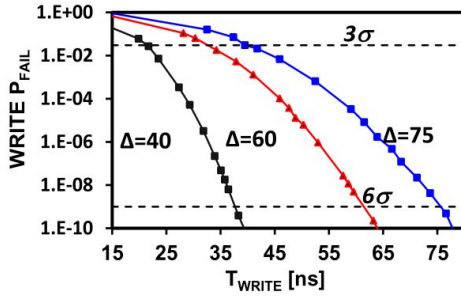


Fig. 18. Write error rate ( $P_{\text{FAIL}}$ ) as a function of the required write time ( $T_{\text{WRITE}}$ ) with  $\Delta = 40, 60, 75$ . The horizontal dashed line labeled as  $6\sigma$  represents the  $6\sigma$ -corner requirement for the write time of a write operation with  $P_{\text{FAIL}} = 10^{-9}$ . Reprinted from [88].

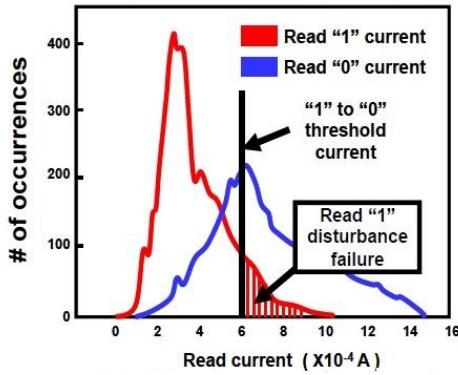


Fig. 19. Read current distribution caused by process variations. The read “1” currents for some worst-case cells exceeding the 1→0 threshold current lead to RDFs. Reprinted from [101].

denoted as  $\langle 0w1/0/- \rangle$  and  $\langle 1w0/1/- \rangle$ , respectively. TFs can be caused by defects as well as extreme process variations. For example, resistive opens along the write current path in Fig. 2(a) lead to a current degradation [88]. As a result, TFs are likely to take place due to a lack of enough current passing through the MTJ device ( $I_w < I_c$ ). Additionally, resistive opens in the word line have an effect of limiting the current driving ability of the access NMOS in bit-cells, thereby leading to TFs.

Process variations may also result in TFs in some cases. As we discussed previously, in order to switch successfully between AP and P states, a write operation has to supply both sufficient amplitude and duration of the write current to overcome the energy barrier between them. In this sense, PV-induced variation in the required switching time ( $t_{\text{sw}}$ ) for individual bit-cells may make some cells subject to TFs since the STT-switching action does not finish within the fixed write time in practical circuit designs ( $t_{\text{sw}} > t_{\text{wr}}$ ). E. Vatajelu et al. referred to this PV-induced TF as *slow write fault* (SWF) [72]. Chintaluri et al. [xxx] observed that write operations are more sensitive to  $V_{\text{th}}$ ,  $t_{\text{ox}}$ , and  $M_s$  than other parameters of the MTJ and transistor. Fig. 18 shows the write error rate of a write operation as a function of the write time for MTJ devices with some given thermal stability values. It can be seen that memory cells with  $\Delta = 40$  require a write time of at least  $\sim 40$  ns to reach a write error rate  $P_{\text{FAIL}} = 10^{-9}$  (equivalent to

$6\sigma$ -corner requirement). In other words, TFs happen to those cells that require more than 40 ns to successfully switch to the other state. As the thermal stability increases, indicating longer retention time, it requires longer write time to maintain the same write error rate. It is worth noting that the continuous technology down-scaling and adoption of PMA-MTJ devices, on one hand, result in a dramatic reduction of the MTJ critical switching current density ( $J_{c0}$ ), which greatly alleviates the TF issue. On the other hand, the probability of read disturbance rises because the gap between the read current  $I_{\text{rd}}$  and the critical switching current  $I_c$  narrows considerably [115].

**Read Destructive Fault (RDF):** this fault arises when a read operation causes an inadvertent flip in the addressed bit-cell. For STT-MRAMs, only RDF1 (denoted as  $\langle 1r1/0/0 \rangle$ ) is possible to occur due to the uni-directional property of read operations, as shown in Fig. 2(d). As  $I_{w0}$  and  $I_{\text{rd}}$  share the same path in the 1T-1MTJ bit-cell structure, a read current is possible to behave as a weak write current and therefore results in an unintended magnetization flip in the FL in the presence of some resistive defects [88]. Apart from defects, process variations are also likely to cause a RDF1. For instance, a low  $R_{\text{AP}}$  of the MTJ, a low  $V_{\text{th}}$  of the NMOS, or a degraded  $\Delta$  elevate the read current  $I_{\text{rd}}$  above the critical switching current  $I_c$  for some worst-case cells, as shown in Fig. 19 [107,116,117]. It is worth noting that RDF0 ( $\langle 0r0/1/1 \rangle$ ) can never happen when the cell is in the P state, since a  $P \rightarrow AP$  transition requires a current flowing from SL to BL whereas a read operation invokes a reversed current.

**Incorrect Read Fault (IRF):** this fault refers to a sensing failure of the actual resistive state in the addressed cell. IRF includes IRF0 and IRF1, which are denoted as  $\langle 0r0/0/1 \rangle$  and  $\langle 1r1/1/0 \rangle$ , respectively. Resistive opens along the read current path can lead to a decrease in the read current. This causes a read operation addressed at a cell with the above defects in the P state to return an incorrect logical value “1” ( $\langle 0r0/0/1 \rangle$ ) [88]. In addition, resistive bridges shorting the SL and the internal node of the memory cell can pull up the read current, therefore leading to a IRF1 ( $\langle 1r1/1/0 \rangle$ ) when the addressed cell is in the AP state.

Process variations also contribute to IRFs. In order to correctly read the resistive state of the MTJ (0 for  $R_P$  and 1 for  $R_{\text{AP}}$ ), a minimal sensing margin is required irrespective of sense amplifier designs. the sensing margin is defined as the gap between the current going through the cell under sensing and the current going through the reference cell. In this regard, a high TMR and less process variations are crucial to guarantee a large sensing margin. However, as technology scales down, the read reliability is increasingly challenging and becoming a bottleneck in STT-MRAM circuit designs. Fig. 20(a) shows the climbing trend of read error rate (i.e., IRF) and the decrease in the as the technology node becomes smaller, caused by deterioration of process variation and TMR parameter [87]. Furthermore, the conflict between read error rate and read disturbance in optimizing read current to achieve better readability, shown in Fig. 20(b), again squeezes the design space for reliable read operations [89].

**Write Disturb Coupling Fault (CFwd):** this fault arises when a write operation on a bit-cell (aggressor) results in



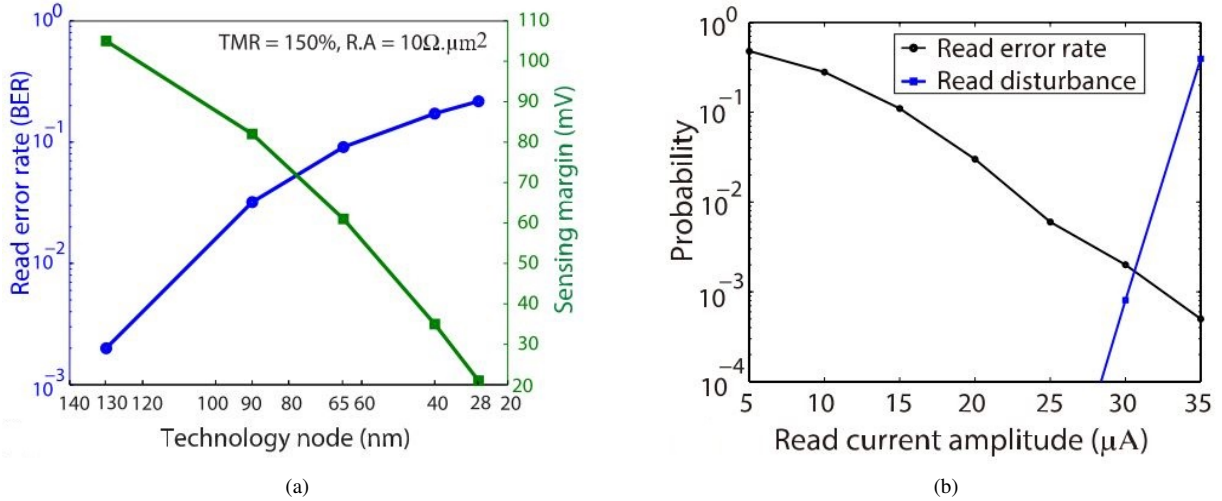


Fig. 20. (a) Read error rate (i.e., IRF) and sensing margin vs. technology scaling. (b) Read error rate and read disturbance (i.e., RDF) vs. read current amplitude at 28nm technology node. Reprinted from [89].

an unintended flip of another bit-cell (victim). Notations for CFwd are  $\langle xw \sim x; 0/1/- \rangle$  or  $\langle xw \sim x; 1/0/- \rangle$  for a transition write on the aggressor cell, and  $\langle xwx; 0/1/- \rangle$  or  $\langle xwx; 1/0/- \rangle$  for a non-transition write on the aggressor cell. For example,  $\langle xw \sim x; 0/1/- \rangle$  means a write operation on the aggressor cell to flip its state from  $x$  to  $\sim x$  inadvertently makes the victim cell flip from 0 to 1. Typical causes of CFwd include the stuck-at-ON defect of the access transistor in the bit-cell, causing an extra write to the victim cell when writing adjacent cells sharing the same BL and SL. Inter-cell bridges between WLs are also reported as the cause of CFwd [88]. It is worth noting that researchers from different institutes use different terminologies to describe CFwd. Chintaluri et al. from Georgia Institute of Technology refer to this fault as a coupling fault [88,96], whereas Vatajelu et al. from TIMA Laboratory (France) call it a write disturb fault [72]. Combining both of them, we believe that the term write disturb coupling fault is more appropriate based on its faulty behavior and causes.

## 2) Transient Faults

We have discussed permanent faults caused by defects and extreme process variations so far. Those faults also exist in conventional memory technologies such as SRAMs and DRAMs. As STT-MRAM is an emerging NVM technology based on many novel physical phenomena, transient faults which are intermittent in some cycles have increasingly been a reliability concern. In this part, we will start with introducing all influential factors that impact the reliability of STT-MRAMs. Thereafter, some resulted transient faults will be discussed.

**Transient Write Fault (TWF):** Due to the stochastic property of STT-switching behavior, the incubation time before the actual start of magnetization precession in the FL varies from one event to the next, as mentioned previously. However, the current pulse width of write operations is generally fixed with some margin over the averaged switching time for STT-MRAM circuit designs in practice. This may lead to an un-

expected write fault when the incubation delay is longer than the given pulse width of write currents. We refer to this fault as *transient write fault* (TWF) in this paper. TWF includes TWF0 and TWF1, which are denoted as  $\langle 0w1/T0/- \rangle$  and  $\langle 1w0/T1/- \rangle$ , respectively.

The major difference between TWF and previous TF is that the former is intrinsically unpredictable and temporary while the latter is deterministic and permanent. Specifically, TWF may happen to all STT-MRAM cells, including those defect-free cells, with a very small probability. It can be self-repaired by the next write operation directly following a faulty one. TF, however, occurs at the cells with some defects or extreme process variations aforementioned, and it always leaves a faulty state in those cells after a transition write operation.

TWF is aggravated by thermal fluctuation, current asymmetry in  $w0$  and  $w1$  operations, and PVT variations [58,118]. First, due to thermal fluctuation, the actual switching time has a wide distribution over cycles; the effects of thermal fluctuation on the STT-induced switching process can be modeled by introducing a thermally-induced random field  $H_{\text{fluc}}$  and an initial angle  $\theta$  between the magnetizations in the FL and the PL (see Equations (9)). Second, the current asymmetry in  $w0$  and  $w1$  operations ( $I_{w0} > I_{w1}$ ), caused by the source degeneration of the access NMOS [57,58], further widens the switching time distribution. Third, the increasing PVT variations with technology downscaling also induce a wide switching time distribution over STT-MRAM cells. Considering above three factors, a large write margin (i.e., a long pulse to cover the wide distribution of the switching time) is required to guarantee a high switching probability for all cells and cycles. However, this comes with the cost of sacrificing write performance and energy. Hence, TWF is increasingly posing a threat to the reliability of STT-MRAM designs.

**Transient Read Disturb Fault (TRDF):** Due to thermal fluctuation, the state of a cell may accidentally flip during a read operation despite the read current is much smaller than the critical switching current [120,121]. We name this

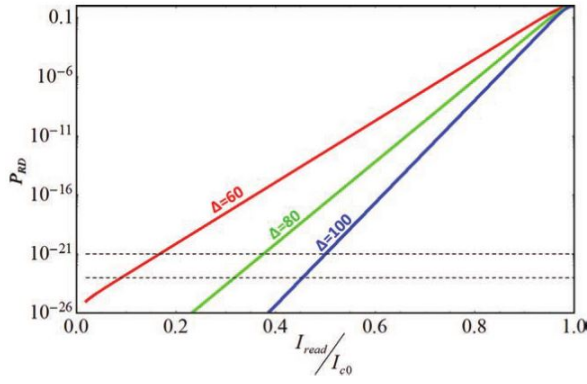


Fig. 21. TRDF probability as a function of read current (10 ns) with respect to various  $\Delta$  values. Typical requirement of TRDF probability is in the range of  $10^{-23}$  to  $10^{-21}$  (the two horizontal dotted lines), setting up a ceiling to the read current value for STT-MRAM cells with various  $\Delta$  values. Reprinted from [119].

fault as *transient read disturb fault* (TRDF). Similar to the aforementioned RDF, only TRDF1 (denoted as  $\langle 1r1/T0/1 \rangle$ ) exists in STT-MRAMs since the read current is uni-directional. Nevertheless, TRDF1 is essentially different from RDF1 which is caused by some defects or extreme process variations, as we discussed previously. First, TRDF1 happens stochastically to all bit-cells, rather than to some cells with defects or extreme PVs, in STT-MRAM chips with a very small probability. The probability of TRDF1 can be approximately calculated by the Neel-Brown model (see Equation (10)). Second, TRDF1 is inherently caused by thermal fluctuation, which is strengthened by applying a read current to the MTJ device due to Joule heating, whereas RDF1 is the result of overdriven read currents, due to defects or extreme PVs. Third, TRDF1 is not reproducible, which means the majority of read 1 operations success without any destruction to the accessed cell while a very small fraction of them end up flipping the cell from 0 to 1 state. By contrast, RDF1 is reproducible meaning that all read 0 or 1 operations lead to a state flip in the target cell. Despite above differences between TRDF1 and RDF1, the prerequisite for them are same:  $I_{w0}$  and  $I_{rd}$  share the same path and the target MTJ device must be in AP state. We give a brief comparison between RDF1 and TRDF1 in Table II.

TRDF in STT-MRAMs can be alleviated by enlarging the gap between the read current and the critical switching current. This can be achieved by either increasing the critical switching current or reducing the read current. Apparently, increasing the critical switching current is not practical because the high write current and power dissipation are already a bottleneck in STT-MRAM designs. In reality, the critical switching current is continually going down as the size of MTJ device shrinks [121]. On the other hand, reducing the read current is a possible solution. But it also squeezes the read margin, posing a threat to the read reliability for sense amplifier designs. Based on Equation (10), one can observe that a shorter read pulse translates to smaller read disturb probability. This can also be considered in practical circuit design while maintaining the effectiveness of sense amplifier voltage development. Despite these possible solutions to reduce the probability of

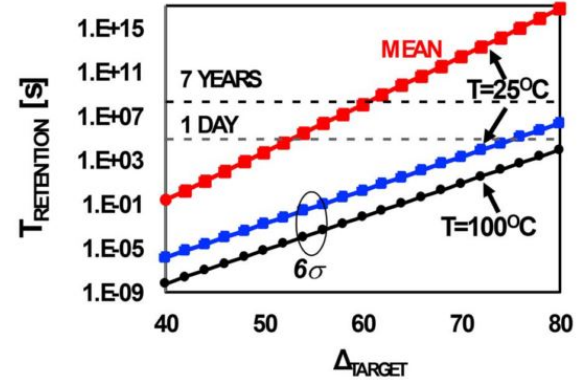


Fig. 22. Retention time vs. target  $\Delta$  value considering process variation (mean and  $6\sigma$  corner) and temperature (25 °C and 100 °C) Reprinted from [88].

TABLE II  
A COMPARISON BETWEEN RDF1 AND TRDF1.

| Fault Models           | RDF1   | TRDF1                      |
|------------------------|--|----------------------------|
| Prerequisite           | 1. $I_{w0}$ and $I_{rd}$ share the same path<br>2. MTJ in AP state |                            |
| Victim Cells           | Cells with defects or extreme PVs                                  | All cells                  |
| Causes                 | $I_{rd} > I_c$   | Thermal fluctuation        |
| Occurrence Probability | Absolute   | Small probability event    |
| Repeatability          | Yes  | No                         |
| Readout data           | Wrong  | Correct                    |
| Notation               | $\langle 1r1/0/0 \rangle$  | $\langle 1r1/T0/1 \rangle$ |

TRDF, it is still going to be a major reliability issue in future technology nodes, as pointed out in [120]. Fig. 21 shows the TRDF probability as a function of read current with a pulse width of 10 ns with respect to various  $\Delta$  values. For a typical requirement of TRDF probability from  $10^{-23}$  to  $10^{-21}$ , the maximum allowed read current is around  $0.1I_{c0}$  for STT-MRAM cells with  $\Delta = 60$ , posing a big challenge to the sense amplifier design in order to obtain reliable and low-latency read operations.

**Retention Fault (RTF):** This fault means a cell loses its content over time, due to thermal fluctuation. RTF includes RTF0 and RTF1 which are denoted as  $\langle 0T/1/- \rangle$  and  $\langle 1T/0/- \rangle$ , respectively. As a static model, Equations (2-4) give an approximation of the retention time for STT-MRAMs. It suggests that RTF exponentially depends on the MTJ dimension and the ambient temperature, but it does not imply the cause of RTF in STT-MRAMs. Unlike the retention fault in DRAMs where the amount of charge on cell capacitors decreases gradually, retention fault in STT-MRAMs takes place instantly (a stochastic process) in the presence of thermal noise [122]. Accordingly, the retention time of every cell in STT-MRAMs is not fixed and predictable in essence. Rather, it fluctuates dynamically depending on the intensity of thermal perturbation. Intel Technology Journal [122] suggests that a bit flip induced by thermal fluctuation has a Poisson distribution with a time characteristic  $\tau_0 e^{\Delta}$ . Thus, the retention fault happens when the bit-cell flips with an odd number of times. If we set  $I = 0$  in Equation (10),  $\tau_1$  now becomes the nominal retention time, and the probability of RTF can be calculated by:

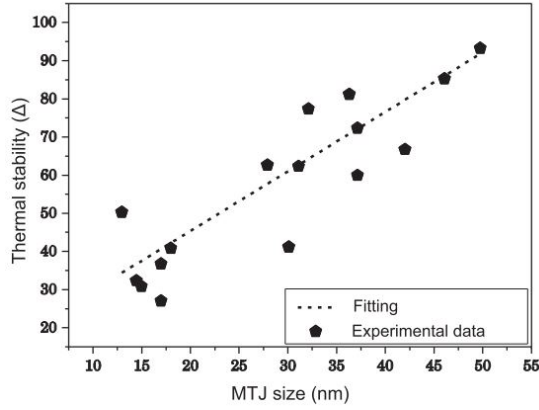


Fig. 23. Experimental measurement and fitting curve of the thermal stability  $\Delta$  with various MTJ sizes. Reprinted from [121].

$$P_{RTF} = 1 - \exp\left(-\frac{t}{\tau_0 \exp(\Delta)}\right), \quad (11)$$

where  $t$  is the observation time window, and  $\tau_0$  is the attempt time ( $\sim 1$  ns).

Furthermore, in the case of  $I \neq 0$  (e.g., during read operations), the thermal fluctuation is strengthened, thus raising the probability of magnetization reversal. Besides, the value of  $\tau_1$  decreases significantly due to the degraded thermal stability  $\Delta_I$  under a read or write current:

$$\Delta_I = \Delta_0 \left(1 - \frac{I}{I_{c0}}\right). \quad (12)$$

This phenomenon can be utilized to experimentally measure the nominal thermal stability (i.e.,  $\Delta_0$  in Equation (12)) of MTJ devices. By repeatedly applying a weak current through the target MTJ device, a statistical probability of magnetization reversal can be obtained to calculate  $\Delta_I$  [123]. Thereafter,  $\Delta_0$  can be calculated based on Equation (12).

Since retention time (i.e., the average lifetime, approximated by Equation (4)) of STT-MRAM cells is exponentially dependent on thermal stability, any factors that degrade  $\Delta$  would reduce the retention time. Obviously, the smaller the  $\Delta$  value, the more vulnerable to RTF. First, an increase in temperature would exponentially boost thermal fluctuation and degrade the  $\Delta$  value, thereby reducing the average retention time as shown in Fig. 13(a). Second, process variations inevitably introduce  $\Delta$  variation among STT-MRAM cells. Fig. 22 shows the retention time as a function of the target  $\Delta$  for mean cells and  $6\sigma$ -corner cells. For STT-MRAM cells with a target  $\Delta$  of 60, the retention time of mean cells is around 7 years under room temperature, but the  $6\sigma$ -corner cells (lower  $\Delta$ ) have a retention time far less than 1 day. If the temperature rises to  $100^\circ\text{C}$ , the retention time becomes even shorter. Third, magnetic coupling is another concern that impacts the thermal stability of memory cells depending on the data pattern in the neighborhood. Fig. 10 shows that the worst data pattern generates a stray field that significantly degrades the  $\Delta$  value at various technology nodes. Fourth, a current flowing through the MTJ device during write and read operations degrades the  $\Delta$  value as well, as seen in Equation (12). Last but not least,

thermal stability decreases as the size of MTJ devices shrinks, as shown in Fig. 23. This is because a smaller FL of the MTJ leads to a lower energy barrier, depicted by Equation (2). Experimental results in [124] show that a 2x shrinkage in the MTJ volume decreases the retention time from a few decades to a few seconds. To obtain the required  $\Delta$  value at advanced technology nodes, the anisotropy field  $H_k$  in the FL of the MTJ must be enhanced, which makes the manufacture of STT-MRAMs become more and more challenging as technology scales down. Due to those influential factors that may degrade the thermal stability of STT-MRAMs, RTF is predicted to be the dominating threat to STT-MRAM reliability at future technology nodes [122].

## V. TEST ALGORITHMS

In this section, we will first discuss March test algorithms proposed in the literature. These March tests can guarantee the detection of certain strong functional fault models such as SAF and TF. Thereafter, we will introduce and compare three test algorithms dedicated to testing the retention time of STT-MRAMs.

### A. March Tests

March tests are commonly used in detecting traditional memory faults, such as SAF, TF, etc., due to their linear complexity, regularity, and symmetry [62]. A March test consists of a finite sequence of march elements, each of which is composed of a sequence of read and/or write operations applied to each memory cell before proceeding to the next. In the literature, there are several papers related to testing MRAMs with March tests.

Chin et al. presented in [125,126] a fault model called write disturb fault (WDF) in toggle MRAMs, where the magnetic field generated in write operations to switch the state of the addressed bit-cell (aggressor) may inadvertently reverse the data stored in adjacent cells (victims). Furthermore, they proposed March C- and March 17N test algorithms to detect SAF, TF, CF, AF, and WDF in their demonstration toggle MRAM chip.

In STT-MRAMs, the cause of WDF is totally different from traditional toggle MRAMs. Rather than induced by writing magnetic field of current-carrying wires in toggle MRAMs, WDF in STT-MRAMs is caused by defects such as access transistor stuck-at-ON or resistive bridges between cells. In this paper, we refer to WDF in STT-MRAMs as write disturb coupling fault (CFwd) as discussed in Section IV-B(1), since it involves more than 1 bit-cell. To detect CFwd as well as SAF, TF, RDF, and IRF in STT-MRAMs, Yoon et al. proposed in [96] a word-oriented March (WOM) test algorithm (26N) as follows.

$$\begin{aligned} &\uparrow (w00); \uparrow (r00, w11, r11); \downarrow (r11, w00, r00); \\ &\downarrow (r00, w11, r11); \downarrow (r11, w00); \uparrow (r00); \\ &\uparrow (r00, w01, r01); \uparrow (r01, w10, r10); \downarrow (r01, w10, r10); \\ &\downarrow (r10, w11, r11); \uparrow (r11) \end{aligned}$$

Recently in ITC2018, Nair et al. reported *dynamic incorrect read fault* (dIRF) based on their circuit simulations. dIRF is an incorrect read fault which is sensitized by at least two consecutive read operations due to a resistive bridge defect between the SL and the internal node of the 1T-1MTJ cell. To detect dIRF, they proposed the following March algorithm (14N).

```

↑ (w0);
↑ (r0, w1, r1, r1, r1, r1);
↓ (r1, w0, r0, r0, r0, r0);
↓ (r0)

```

### B. Retention Time Tests

In Section IV-B(2), we have discussed the characteristics, causes, and influencing factors of retention fault in STT-MRAMs. Yet, the requirement of retention time for STT-MRAMs ranges from a few seconds to ten years, depending on the specific application. For the storage-class memory (SCM) application, 10+ years of retention time is desired as most of the data is rarely revisited. This requires a thermal stability ( $\Delta$ ) as high as 80, which is experimentally achievable at the expense of high write energy and latency. In contrast, for the last-level-cache application which is seen as one of the most important markets for applying STT-MRAM technology in the short term, the average revival time of cache blocks is below 1 s [5]. This allows us to trade the retention time of STT-MRAMs for better write performance, which has been extensively studied [127–129].

Regardless of the different requirements of retention time of STT-MRAMs for different applications, testing retention time of STT-MRAMs is very important. However, characterizing STT-MRAM retention time is very challenging, since retention fault is essentially a transient and stochastic fault which depends on temperature, process variations, magnetic perturbation, and disturb current. Thus, March tests are not suitable to test it, and traditional retention tests for DRAMs cannot be directly applied to STT-MRAMs. This calls for special test techniques. Next, we will introduce three test approaches dedicated to testing STT-MRAM retention time.

#### 1) Statistic method With a Weak Disturb Current

Intel proposed a method to test the retention time of STT-MRAM cells by applying a weak disturb current through them [122]. Equation (10) can be used to calculate the switching probability in the thermal activation regime under a long ( $t_p$ ) but weak write current ( $I_{\text{wwr}} < I_{c0}$ ). In this case, we derive:

$$\frac{t_p}{\tau_0 \exp(\Delta(1 - I_{\text{wwr}}/I_{c0}))} \ll 1. \quad (13)$$

By performing Taylor expansion, we can derive the following expression:

$$\ln(\text{Pr}(I_{\text{wwr}})) = \ln\left(\frac{t_p}{\tau_0}\right) - \Delta\left(1 - \frac{I_{\text{wwr}}}{I_{c0}}\right). \quad (14)$$

Equation (14) links the *disturb probability*  $\text{Pr}(I_{\text{wwr}})$  with the thermal stability  $\Delta$  under a long but weak write current.

#### Algorithm 1 Retention time based on weak disturb current.

---

**Input:**  $I_{\text{wwr}}[N]$  = array containing N number of  $I_{\text{wwr}}$  values  
**Input:**  $t$  = the current pulse width of  $I_{\text{wwr}}$   
**Input:**  $M$  = the number of experiments for each  $I_{\text{wwr}}$  value  
**Output:** Retention time for a cell

---

```

Initialization
for i = 0 to N - 1 do
    Regular write of a test pattern
    for j = 0 to M - 1 do
        Weak write with current  $I_{\text{wwr}}[i]$  for time  $t$ 
        Regular read
        if readout data  $\neq$  test pattern then
            Error counter ++
            Rewrite the test pattern
        end if
    end for
    Pr[i] = Error counter/M
    Reset error counter
end for
Extrapolation of  $\Delta$  with equation (14)
Approximation of  $T_{\text{ret}}$  with equation (4)
return  $T_{\text{ret}}$ 

```

---

This equation can be used to experimentally measure the  $\Delta$  value. By repeatedly applying a large number of weak write currents (e.g.,  $I_{\text{wwr}} < 0.8I_{c0}$ ,  $t = 100$  ns) to the memory cell under test, we can obtain a statistic result for  $\text{Pr}(I_{\text{wwr}})$ . Thereafter,  $\Delta$  value can be derived with Equation (14). As the retention time is exponentially dependent on  $\Delta$ , it can thus be approximated according to Equation (4). The complete test process is described with Algorithm 1.

Though theoretically feasible, the test time using this method is prohibitive in practice. In order to get a statistic result for the  $\text{Pr}(I_{\text{wwr}})$  with a 1% error margin,  $5 \times 10^5$  number of tests are needed for each data point assuming that the expected probability is  $1 \times 10^{-3}$ . Consequently, it takes approximately 0.5 s to test a bit-cell and more than 5 days to test a 64-MB array [122]. Note that this is only the time spent on estimating the  $\text{Pr}(I_{\text{wwr}})$  for all cells in the array without taking into account the subsequent calculation of  $\Delta$  and retention time. Worse still, the test time increases with the array size and  $\Delta$  value. Hence, this is obviously unacceptable from the perspective of test time.

#### 2) Burn-in Methods

To reduce the prohibitive test time of retention time in STT-MRAMs, Burn-in test techniques to compress the retention time is an effective way. Since the thermal stability  $\Delta$  of the MTJ device significantly depends on ambient conditions such temperature, magnetic field, and disturb current, it is viable to change those conditions to compress the  $\Delta$  value, thus accelerating the process of retention fault. Combining Equations (3, 7, 12), we derive the following equation:

$$\Delta(T, I, H_{\text{offset}}) = \frac{E_B}{k_B T} \left(1 - \frac{I}{I_{c0}}\right) \left(1 - \frac{H_{\text{offset}}}{H_k}\right)^2. \quad (15)$$

Equation (15) indicates that an increase in temperature  $T$  leads to a smaller  $\Delta$  value. Moreover, The  $\Delta$  value decreases with



**Algorithm 2** Burn-in retention test based on binary search.**Input:**  $N_{\text{seh}}$  = the number of binary searches for averaging**Input:**  $N$  = iterations in a search**Input:**  $t_{\text{UB}}$  = upper bound of the predicted retention time**Input:**  $t_{\text{LB}}$  = lower bound of the predicted retention time**Output:** Retention time for an STT-MRAM cell

Initialization

**for**  $i = 0$  to  $N_{\text{seh}} - 1$  **do** $t_{\text{ret}}[i] = 1/2 \times (t_{\text{UB}} + t_{\text{LB}})$ **for**  $j = 0$  to  $N - 1$  **do**Regular write of a *test pattern*Wait for time  $t_{\text{ret}}[i]$ Regular read for a *readout data***if** *readout data*  $\neq$  *test pattern* **then** $t_{\text{UB}} = t_{\text{ret}}[i]$ **else** $t_{\text{LB}} = t_{\text{ret}}[i]$ **end if** $t_{\text{ret}}[i] = 1/2 \times (t_{\text{UB}} + t_{\text{LB}})$ **end for** $T_{\text{ret}} = \sum_{N_{\text{seh}}} t_{\text{ret}}[i]$ **end for****return**  $T_{\text{ret}}$ 

a current  $I$  flowing through the MTJ device and an external offset field  $H_{\text{offset}}$  opposite to the intrinsic anisotropy field  $H_k$  of the FL. Ghosh et al. [124] proposed two algorithms to test the retention time of STT-MRAM cells with a thermal burn-in scheme, whereby the retention time can be  $1000\times$  smaller when the temperature rises to  $125^\circ\text{C}$ .

The first algorithm is named as binary-search-based retention test, as depicted in Algorithm 2. This algorithm describes the process of testing the retention time ( $T_{\text{ret}}$ ) of a single bit-cell. Initially, a lower bound search time ( $t_{\text{LB}}$ ) and an upper bound search time ( $t_{\text{UB}}$ ) for the retention time are selected according to the predicted thermal stability of STT-MRAM arrays under test. Thereafter a test data pattern is written into the first memory cell under test, followed by a fixed period of wait time ( $t_{\text{ret}}$ ), equal to the mean of  $t_{\text{LB}}$  and  $t_{\text{UB}}$ . After the wait time, the data in this cell is read out and compared with the original test pattern. If they are the same, meaning no retention fault occurs, the  $t_{\text{LB}}$  value is updated with the wait time  $t_{\text{ret}}$ . If not, the  $t_{\text{UB}}$  value is updated with the  $t_{\text{ret}}$ . As this process iterates, the  $t_{\text{ret}}$  value gradually approaches the actual retention time of the cell under test. Depending on the accuracy we desire, the overall test time increases with the number of binary searches for averaging and the iteration cycles in each search.

The second algorithm searches the retention time in a linear way, described below in Algorithm 3. With this algorithm, the time step ( $T_{\text{step}}$ ) in each search and the number of searches ( $N_{\text{seh}}$ ) are given to determine the search resolution and test accuracy, respectively. The test starts with a regular write of a given test data pattern into the cell under test. Then it periodically reads the data back with the time step  $T_{\text{step}}$  to compare it with the original data pattern. This search process proceeds until a mismatch is observed, similar to the polling

scheme in CPU. Clearly, a small time step results in a high test accuracy at the expense of more read operations.

**Algorithm 3** Burn-in retention test based on linear search.**Input:**  $N_{\text{seh}}$  = the number of linear searches for averaging**Input:**  $T_{\text{step}}$  = resolution of the retention time test**Output:** Retention time for an STT-MRAM cell

Initialization

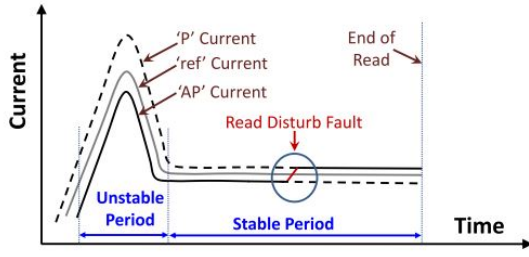
**for**  $i = 0$  to  $N_{\text{seh}} - 1$  **do**Regular write of a *test pattern*Reset *step counter***while** *readout data* = *test pattern* **do**Wait for time  $T_{\text{step}}$ *step counter*++Regular read for a *readout data* $t_{\text{ret}}[i] = T_{\text{step}} \times \text{step counter}$ **end while****end for** $T_{\text{ret}} = \sum_{N_{\text{seh}}} t_{\text{ret}}[i]$ **return**  $T_{\text{ret}}$ 

## 3) Algorithm Comparison

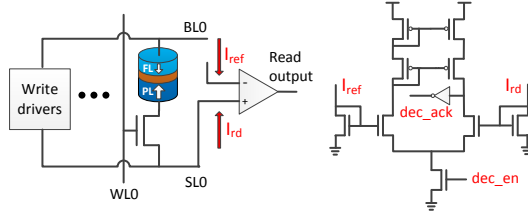
As aforementioned, the statistical method based on the injection of a weak disturb current in Algorithm 1 is extremely time-consuming, due to the low occurrence rate of the retention fault at room temperature. Algorithm 2 and 3 can be superior to Algorithm 1 if the compression rate is very high such that the compressed retention time is on the order of ms or below. This is applicable to STT-MRAMs with a low  $\Delta$  for cache applications, where the averaged block lifetime is below 1s. However, for SCM applications requiring 10+ years of retention time, it is of no avail to compress and test the retention time with a linear search or a binary search. For instance, compared to 0.5s for testing a bit-cell with  $\Delta = 60$  using Algorithm 1, Algorithm 2 or 3 takes more than  $10\times$  test time even with a compression rate as high as  $10^8$  combining both the thermal burn-in and the disturb current techniques, as claimed in [124]. Under such a high compression rate, the resulted retention time is approximately 3s, which is the minimum test time for a bit-cell using Algorithm 2 or 3. Therefore, there is still space to explore for testing the retention time of STT-MRAMs in a cost-efficient way for various applications. One possible solution is to combine the following three burn-in techniques to aggressively compress the thermal stability  $\Delta$ : 1) thermal burn-in with an elevated temperature; 2) electrical burn-in with the injection of a weak disturb current; 3) magnetic burn-in with an external magnetic field  $H_{\text{offset}}$  opposite to the intrinsic anisotropy field  $H_k$  of the FL.

## VI. DESIGN FOR TESTABILITY

As aforementioned, permanent fault models such as SAF and TF in STT-MRAMs can be detected by March tests. However, March tests cannot guarantee the detection of STT-MRAM transient faults (i.e., TWF, TRDF, and RTF) which only take place in some specific cycles with certain occurrence rates. Thus, transient faults require *design-for-testability* (DfT)



(a) Illustration of the abrupt current increase due to the occurrence of TRDF while reading 1(AP) state. Reprinted from [120].



(b) Bit-flip detection circuit by means of comparing the read current ( $I_{rd}$ ) going through the cell under read and the current ( $I_{ref}$ ) flowing through the reference cell [120].

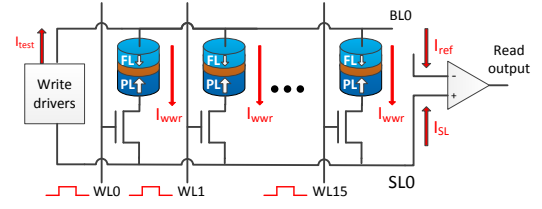
Fig. 24. Design for TRDF detection: (a) principle, and (b) circuit design.

techniques for detecting them. In this section, we will discuss two circuit designs proposed in the literature for the detection of TRDF and RTE.

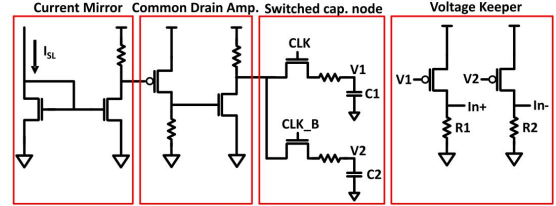
#### A. Design for TRDF Detection

Transient read disturb fault (TRDF) in STT-MRAMs is a transient fault and is increasingly becoming a threat to the reliability of STT-MRAMs, as we discussed previously. Thus, developing DfT designs to facilitate TRDF detection has received great attention. Two similar circuit-level DfT techniques have been proposed separately in [120,121] to detect TRDF. Both of them are based on a key observation: TRDF changes the MTJ resistance of the victim cell, which in turn affects the current amplitude during read operations.

Fig. 24(a) illustrates that the read current goes up abruptly from below  $I_{ref}$  to above  $I_{ref}$  when a TRDF occurs during a read 1(AP) operation. The solid gray line indicates the current flowing through the reference cell during read operations, and the dashed lines below and above the solid gray line indicate the currents flowing through fault-free cells in AP state and P state, respectively. The solid black line indicates the actual current change over time in a read operation during which a TRDF (marked with the blue circle) takes place. This observation is leveraged to detect TRDF by integrating a dedicated circuit into the sense amplifier to track the current change in read operations. Fig. 24(b) shows the bit-flip detection circuit design. The  $dec\_en$  signal is only asserted when reading 1(AP) state. In this case, two current mirrors are used to copy the current  $I_{rd}$  going through the cell under read and the current  $I_{ref}$  flowing through the reference cell from the inputs of the sense amplifier. As long as  $I_{rd}$  is smaller than  $I_{ref}$ , the disturb acknowledgment signal  $dec\_ack$  remains at “0” state. However, if  $I_{rd}$  increases abruptly above  $I_{ref}$  (i.e., TRDF



(a) Repeatedly applying weak write currents to 16 rows of cells simultaneously in test mode to get statistical estimation of  $Pr(I_{wwr})$ .



(b) Tracking the current on the SL ( $I_{SL}$ ) during tests so as to avoid unnecessary read operations when no bit flip occurs [96].

Fig. 25. Retention test implementation: (a) measurement of read disturb probability  $Pr(I_{wwr})$ , and (b) bit-flip detection circuit.

occurs) in the stable period of the sensing process, the  $dec\_ack$  signal immediately makes a transition to “1” state, indicating a detection of TRDF. Despite the effectiveness of detecting TRDFs by means of this technique at the expense of negligible power and area overhead, neither of the two papers provides further insights into how to repair or tolerate TRDF in STT-MRAMs.

#### B. Design for Retention Test

In order to test the retention time of STT-MRAM cells more efficiently, Yoon et al. improved Algorithm 1 and implemented a memory build-in-self-test (MBIST) [96,130]. As aforementioned, Algorithm 1 has many limitations including: 1) the retention test has to be carried out in an operating region where the switching probability  $Pr(I_{wwr})$  is very small under a small current  $I_{wwr}$ ; 2) the majority of read operations after applying the weak write current are not necessary due to the small switching probability; 3) the test time is prohibitive and increases with  $\Delta$  value and array size. To overcome these limitations, the MBIST implementation leverages the philosophy behind the preceding TRDF detection to avoid unnecessary read operations when the retention fault does not occur. In addition, applying the weak write current to multiple rows simultaneously instead of a single row in Algorithm 1 within a test iteration significantly speeds up the test process.

The retention test process starts with writing a predefined data pattern into the cells under test. The data pattern is set to 1 due to two considerations. First, the small current disturbance is uni-directional (i.e., from AP state to P state). Second, the thermal stability is at the lowest value when the cell is in AP state due to the inter-cell magnetic coupling among neighboring cells as we discussed in Section III-C. Thereafter, a weak write current ( $I_{wwr}$ ) is applied to 16 rows of cells at the same time, as illustrated in Fig. 25(a). By tracking the current change on the SL using a dedicated bit-flip detection

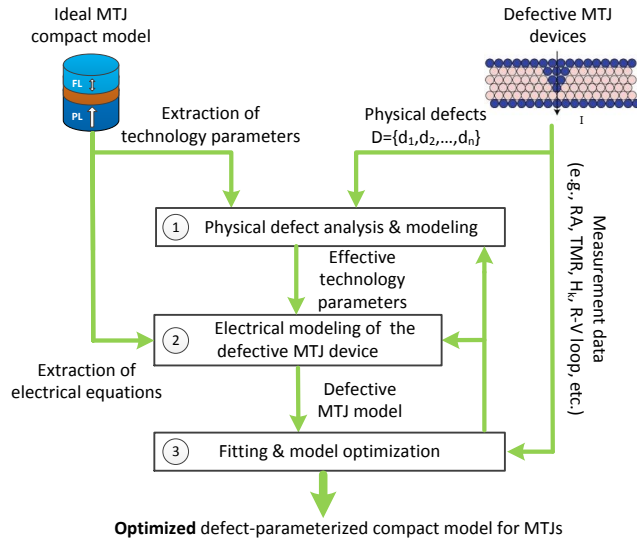


Fig. 26. Electrical modeling flow for STT-MRAM-specific defects.

circuit (see Fig. 25 (b)), a bit-flip can be immediately detected as  $I_{SL}$  increases slightly when any cell among the 16 cells flips from AP state to P state. The slight increase in  $I_{SL}$  is first amplified by a current mirror and transferred to voltage difference, which is further amplified by a multi-stage common drain amplifier. Thereafter, the switched capacitors C1 and C2 sample the voltage alternatively based on the CLK and CLK\_B signals. At the end of this chain, a voltage keeper is used to make sure the voltage difference between the In+ and In- nodes is always higher than 10 mV to avoid metastability. When the sense amplifier is enabled, the voltage difference between the In+ and In- nodes is fully amplified to VDD and GND.

With this scheme for the retention test, experimental results in [96] show a 93.75% improvement in test time compared to the conventional test scheme based on Algorithm 1.

## VII. DISCUSSION

As one of the most promising NVM technologies, STT-MRAM offers competitive write performance, endurance and data retention. The tunability of these three aspects also makes it customizable for a variety of applications such as last-level caches, Internet-of-Things, and automotive. Therefore, STT-MRAM has received a large amount of investment from major semiconductor companies including Intel and Samsung, which have demonstrated its manufacturability in recent years. However, several challenges remain to be addressed before its mass production at different levels, including failure mechanisms, fault modeling, and test development. In this section, we will discuss the key challenges at these three levels.

### A. Challenges for Failure Mechanisms

In Section III, we have discussed the main failure mechanisms for STT-MRAM, namely manufacturing defects, extreme process variations, magnetic coupling, STT stochastic switching, and thermal fluctuation. Next, we discuss the remaining challenges for these failure mechanisms.

First, the cause, location, occurrence rate, and electrical impact of STT-MRAM manufacturing defects have not been fully explored yet. We have collected and presented in this survey all potential manufacturing defects reported in the literature especially for those related to the fabrication of MTJ devices which are the data-storing elements for STT-MRAMs. However, more research work needs to be done in terms of investigating the characteristics of each defect in STT-MRAMs. For example, physical measurement (e.g., TEM) of the defect sheds light on the cause and location; this is important to understand how and where the defect is introduced. In addition, investigating the occurrence rate of each defect indicates how important the defect is. Last but not least, electrical characterization of defects especially those occurred in the MTJ device is also crucial to understand the electrical consequence at memory-cell level.

Second, developing accurate models for STT-MRAM-specific defects is still a challenge. Conventionally, physical defects are modeled as resistive shorts and opens which are used to develop fault models based on circuit simulations. Although this defect modeling approach is still qualified to model defects in interconnects of STT-MRAMs, it may not be applicable for defects in MTJ devices. In our recent work [131], we demonstrated with silicon measurement data that using linear resistors to model pinhole defects in the MgO tunnel barrier of MTJ devices is inaccurate. This is due to the fact that linear resistors cannot capture defect-induced changes in magnetic properties, which are as important as electrical ones for MTJ devices. Furthermore, inaccurate defect modeling may result in incorrect fault models, leading to low-quality test solutions for non-existing problem. Therefore, it is paramount to understand the physics of STT-MRAM-specific defects so as to provide accurate defect models. This is important to guarantee a high-quality test solution as well as to improve the manufacturing process itself so as to improve yield. In [132], we proposed a three-step defect modeling methodology, where the effects of physical defects on the MTJ device are incorporated into the technology parameters of the MTJ device and thereafter on its electrical parameters, as shown in Fig. 26. It is worth-noting that measurement data of real defective MTJ devices is a vital to ensure the accuracy of the defect models for a specific STT-MRAM design and manufacturing process.

Third, with technology downscaling, the unique failure mechanisms in STT-MRAMs such as magnetic coupling, STT stochastic switching, and thermal fluctuation are increasingly become reliability issues. As discussed previously, these new failure mechanisms result in transient faults (e.g., TWF, TRDF) which intermittently appear in some specific cycles during usage. This has been one of the major obstacles limiting the mass commercialization of STT-MRAM in the industry. To reach desired write error rate and read error rate meeting the industry's standards, mitigation techniques are required at device, circuit, and system levels. For example, at device level, the double SAF structure of MTJ stack was reported to be effective in compensating the offset field  $H_{offset}$  at the FL [107,133]. In addition, innovations on MTJ stack designs to further cut down the switching current below 100  $\mu$ A while

maintaining a fast switch speed for sub-10 ns are also urgently needed [134]. At circuit level, a large write margin (i.e., higher write current amplitude and duration) can be employed to ensure a high switching probability of the state in MTJ devices from a circuit design perspective. Another example of circuit-level techniques is write-verify-write scheme which has been adopted by Intel in [11]. In this scheme, a read operation is applied immediately following a write operation to verify whether or not the write operation is successful. If failed, a second write operation is required to write the same data again in order to guarantee the data has been successfully written to the addressed cell. However, these two circuit-level techniques come at the expense of higher energy consumption and performance loss. At system level, error correction codes (ECCs) are commonly used to tolerate some bits of transient faults at run time by introducing redundant parity bits. Nevertheless, strong ECCs are also costly, as the area and latency overhead greatly increases with the number of correction bits.

### B. Challenges for Fault Modeling

As introduced in Section IV, permanent faults in STT-MRAMs are induced by manufacturing defects and extreme process variations while transient faults are caused by magnetic coupling, STT stochastic switching, and thermal fluctuation. Both permanent and transient faults are the high-level representation of failure mechanisms. Thus, it is of great importance to develop accurate fault models reflecting the physical natures of above-mentioned failure mechanisms. Next, we discuss challenges in terms of fault modeling for STT-MRAMs.

First, a consistent fault nomenclature is necessary to unify all existing fault terminologies. At present, the names of fault models for STT-MRAMs in the literature are chaotic and ambiguous. This can be reflected at three aspects as follows.

- Current fault model names are not intuitively interpretable. For instance, Vatajelu et al. [72] defined the transient write fault caused by the STT stochastic switching property as undefined write fault (UWF). However, this name does not imply the transient attribute meaning that this fault only occurs in some cycles with certain probability during run time. Furthermore, the term “undefined” here is rather ambiguous, as UWF in RRAM means that the cell resistance is settled to an intermediate (undefined) state between logic 0 and 1.
- The same fault model name describes different faulty behaviors. For example, TRDF differs from RDF in terms of physical causes, repeatability, and readout data, etc., as shown in Table II. Moreover, RDF is a type of permanent faults which should be targeted during manufacturing tests, while TRDF is transient thus needs to be excluded during manufacturing tests. However, these two different faults are both referred to as read disturb/destructive fault in the literature.
- The same faulty behavior is named differently among different researchers. As discussed in Section IV.B, transition fault is also named as slow write fault, and write

disturb coupling fault is named as coupling fault or write disturb fault by different researchers. The chaos in terminology usage may impede the communication and collaboration in the test community.

Second, a systematic fault analysis methodology is required. Conventionally, fault analysis is based on circuit simulation with the injection of resistive defects (i.e., opens and shorts); the defect strength is determined by the resistance of the injected linear resistors. Thereafter, fault models are proposed to describe the resultant faulty behaviors. This method however has limitations as follows.

- Some of the fault models developed with the conventional linear-resistor-based defect modeling approach may not exist in practice. As afore-mentioned, defects in MTJ devices require a more accurate defect modeling approach to capture the changes in both the device’s magnetic and electrical properties. Using linear resistors to model those defects may results in wrong fault models which do not exist in practice, leading to an inefficient test solution.
- The current expression of faulty behaviors is not rigorous and systematic. As it can be observed in the papers related to STT-MRAM testing, memory fault behaviors are described by fault models; their names indicate the corresponding fault behaviors. This fault description method is not easily interpretable from the name itself, and it can be even confusing sometimes. One example is the previously-discussed undefined write fault UWF where the exact fault behavior is not very clear to a reader. In our latest paper [135], we defined the complete fault space and nomenclature, qualified to describe all faults in STT-MRAMs.
- The fault analysis is not complete and systematic. As discussed in Section IV-B, the state-of-the-art of fault modeling for STT-MRAMs is limited to static faults in STT-MRAM cell array. However, memory cells with defects which do not sensitize any static faults are not necessarily fault-free. Dynamic faults [136] which are sensitized by more than one operations should also be considered in the fault analysis. Furthermore, even if a small defect does not sensitize any static faults or dynamic faults, it may cause weak faults, leading to a shorter lifetime or higher in-field failure rate. Thus, attention should also be paid to those weak faults especially when it comes to defective-part-per-billion (DPPB) level test requirement. Moreover, faults located in address decoders and read&write circuits are also need to be covered, since these peripheral circuits are indispensable for STT-MRAM chips but may also subject to manufacturing defects.

### C. Challenges for Test/DfT Development

Test algorithms and DfT designs targeting STT-MRAMs are still not established yet. Research in this field is ongoing to guarantee a high percentage of defect/fault coverage meanwhile minimizing the test cost and time. For strong faults (including static and dynamic faults) which can be sensitized by a sequence of read/write operations, March tests are typically used to detect them. For weak faults, DfT designs



are needed to guarantee the detection. To ensure a high-quality test solution for STT-MRAMs, the following issues need to be addressed.

First, an effective and efficient March test necessitates accurate fault models. Since fault models are the targets of March tests, unrealistic fault models may result in a poor-quality March test for non-existing problem, meaning a waste of time. Worse still, test escape can happen when manufacturing defects are not well modeled and detected by the test.

Second, transient faults should be excluded somehow during manufacturing tests. As discussed in Section IV-B, transient faults are mainly caused by magnetic coupling, STT stochastic switching, and thermal fluctuation. They do not appear in every cycle and can be self-corrected or tolerated by circuit/system level techniques such as ECCs. Therefore, manufacturing tests should target permanent faults rather than transient faults. However, given the high requirement on the time and cost for mass production tests, transient faults may show up in good devices during tests, causing overkilling good chips. This is known as yield loss. Therefore, it is of great importance to distinguish transient faults from permanent faults during manufacturing tests to avoid failing good chips.

Third, STT-MRAM retention test is extremely time consuming especially for those chips for storage applications requiring a retention time of >10 years. This makes integrating retention test to production tests (where every fabricated chip is tested) prohibitively expensive, similar to other burn-in/stress tests. In Section V-B and VI-B, three test algorithms along with a DfT design for STT-MRAM retention test have been introduced, but none of them is as cost-efficient as desired in practice. To further reduce the retention test time, stress tests such as magnetic burn-in, thermal burn-in, and disturb current application, along with DfT designs provide a feasible solution.

## VIII. CONCLUSION

This paper surveys the state-of-the-art on STT-MRAM testing at three abstraction levels, namely failure mechanisms, fault models, and tests. We presents that manufacturing defects, extreme process variations, magnetic coupling, STT-switching stochasticity, and thermal fluctuation are the main failure mechanisms for STT-MRAMs. To ensure a good test solution, it is paramount to understand these failure mechanisms so as to propose accurate model for them. Special attentions should be paid to the defects in MTJ devices which are the data-storing elements in STT-MRAMs. Rather than modeling those MTJ-related defects as linear resistors conventionally, it is necessary to open the black box of the MTJ model and incorporate the physical defects into the device model. Accurate fault modeling requires both accurate defect models and a systematic fault analysis methodology. The proposed test algorithms and DfT designs in the literature are very limited and the effectiveness is still in doubt. A cost-efficient March test is required to detect permanent faults while excluding transient faults. Meanwhile, DfT designs or stress tests such as magnetic and thermal burn-in are also need to be taken into account to detect weak faults especially when considering high test requirements toward DPPB level. As STT-MRAM testing

is still an emerging research topic, manufacturing tests are far from well established yet. Therefore, more research work needs to be done on this topic to address remaining challenges at these three abstraction levels.

## REFERENCES

- [1] Y. Chen *et al.*, "Recent technology advances of emerging memories," *IEEE Design & Test*, vol. 34, pp. 8–22, 2017, doi:10.1109/MDAT.2017.2685381.
- [2] A. Chen, "A review of emerging non-volatile memory (NVM) technologies and applications," *Solid-State Electronics*, vol. 125, pp. 25–38, 2016, doi:10.1016/j.sse.2016.07.006.
- [3] S. Yu and P.Y. Chen, "Emerging memory technologies: recent trends and prospects," *IEEE Solid-State Circuits Magazine*, vol. 8, pp. 43–56, 2016, doi:10.1109/MSSC.2016.2546199.
- [4] C.J. Xue *et al.*, "Emerging non-volatile memories: opportunities and challenges," in *IEEE Int. Conf. Hardware/Software Codesign and System Synthesis*, 2011, doi:10.1145/2039370.2039420.
- [5] A. Jog *et al.*, "Cache revive: architecting volatile STT-RAM caches for enhanced performance in CMPs," in *Proc. Design Automation Conference*, 2012, doi:10.1145/2228360.2228406.
- [6] X. Fong *et al.*, "Spin-transfer torque memories: devices, circuits, and systems," *Proc. IEEE*, vol. 104, pp. 1449–1488, 2016, doi:10.1109/JPROC.2016.2521712.
- [7] A. Driskill-Smith, "Latest advances and future prospects of STT-RAM," in *Non-Volatile Memories Workshop*, 2010, [http://nvmw.eng.ucsd.edu/2010/documents/Driskill-Smith\\_Alexander.pdf](http://nvmw.eng.ucsd.edu/2010/documents/Driskill-Smith_Alexander.pdf).
- [8] J.J. Kan *et al.*, "Systematic validation of 2x nm diameter perpendicular MTJ arrays and MgO barrier for sub-10 nm embedded STT-MRAM with practically unlimited endurance," *IEEE Int. Electron Devices Meeting*, pp. 27.4.1–27.4.4, 2016, doi:10.1109/IEDM.2016.7838493.
- [9] J.M. Slaughter *et al.*, "High density ST-MRAM technology (invited)," in *IEEE Int. Electron Devices Meeting*, Dec. 2012, doi:10.1109/IEDM.2012.6479128.
- [10] Electronicdesign, "The industrys first 1Gb pMTJ-based STT-MRAM," accessed in Nov. 2016, <http://electronicdesign.com/products/industry-first-1gb-ddr4-perpendicular-st-mram-device-introduced>.
- [11] O. Golonzka *et al.*, "MRAM as embedded non-volatile memory solution for 22FFL FinFET technology," in *IEEE Int. Electron Devices Meeting*, 2018, doi:10.1109/IEDM.2018.8614620.
- [12] Y.J. Song *et al.*, "Demonstration of highly manufacturable STT-MRAM embedded in 28nm logic," in *IEEE Int. Electron Devices Meeting*, 2018, doi:10.1109/IEDM.2018.8614635.
- [13] S. Hamdioui *et al.*, "Test and reliability of emerging non-volatile memories," *IEEE 26th Asian Test Symposium*, pp. 175–183, 2017 doi:10.1109/ATS.2017.42.
- [14] Y. Huai, "Spin-transfer torque MRAM (STT-MRAM): challenges and prospects," *AAPPS Bulletin*, vol. 18, 2008, <https://pdfs.semanticscholar.org/0322/c80c8b69d4efb256482165da7e230752ef43.pdf>.
- [15] M. Gajek *et al.*, "Spin torque switching of 20nm magnetic tunnel junctions with perpendicular anisotropy," *Applied Physics Letters*, vol. 100, p. 132408, 2012, doi:10.1063/1.3694270.
- [16] S. Yuasa *et al.*, "Giant room-temperature magnetoresistance in single-crystal Fe/MgO/Fe magnetic tunnel junctions," *Nature materials*, vol. 3, pp. 868–871, 2004, doi:10.1038/nmat1257.
- [17] S. Ikeda *et al.*, "A perpendicular-anisotropy CoFeB-MgO magnetic tunnel junction," *Nature Materials*, vol. 9, pp. 721–724, 2010, doi:10.1038/nmat2804.
- [18] A. Manchon *et al.*, "Analysis of oxygen induced anisotropy crossover in Pt/Co/MoX trilayers," *Journal of Applied Physics*, vol. 104, p. 043914, 2008, doi:10.1063/1.2969711.
- [19] M. Nakayama *et al.*, "Spin transfer switching in Tb-CoFe/CoFeB/MgO/CoFeB/TbCoFe magnetic tunnel junctions with perpendicular magnetic anisotropy," *Journal of Applied Physics*, vol. 103, pp. 07A710–07A710, 2008, doi:10.1063/1.2838335.
- [20] M. Krounbi *et al.*, "Status and challenges in spin-transfer torque MRAM technology," *ECS Transactions*, vol. 69, pp. 119–126, 2015, <http://ecst.ecsdl.org/content/69/3/119.full.pdf>.
- [21] H. Jin and T. Miyazaki, "Tunnel magnetoresistance effect," in *The Physics of Ferromagnetism*. Springer Series in Materials Science, 2012, vol. 158, pp. 403–432, doi:10.1007/978-3-642-25583-0\_12.
- [22] S. Yuasa *et al.*, "Giant room-temperature magnetoresistance in single-crystal Fe/MgO/Fe magnetic tunnel junctions," *Nature Materials*, vol. 3, pp. 868–871, 2004, doi:10.1038/nmat1257.

- [23] a.V. Khvalkovskiy *et al.*, “Basic principles of STT-MRAM cell operation in memory arrays,” *Journal of Physics D: Applied Physics*, vol. 46, p. 074001, 2013, doi:10.1088/0022-3727/46/7/074001.
- [24] D. Apalkov, B. Dieny, and J.M. Slaughter, “Magnetoresistive random access memory,” *Proc. IEEE*, vol. 104, pp. 1796–1830, 2016, doi:10.1109/JPROC.2016.2590142.
- [25] N. Strikos *et al.*, “Low-current probabilistic writes for power-efficient STT-RAM caches,” in *IEEE Int. Conf. Computer Design*, Oct. 2013, doi:10.1109/ICCD.2013.6657095.
- [26] Y. Huai *et al.*, “Observation of spin-transfer switching in deep submicron-sized and low-resistance magnetic tunnel junctions,” *Appl. Phys. Lett.*, vol. 84, pp. 3118–3120, 2004, doi:10.1063/1.1707228.
- [27] J. Slaughter *et al.*, “Toggle and spin-torque MRAM: status and outlook,” *J. Magnetic Society of Japan*, vol. 5, p. 171, 2010, [https://www.everspin.com/sites/default/files/WP\\_Toggle\\_and\\_ST\\_MRAM\\_Status\\_and\\_Outlook.pdf](https://www.everspin.com/sites/default/files/WP_Toggle_and_ST_MRAM_Status_and_Outlook.pdf).
- [28] A. Driskill-Smith *et al.*, “Latest advances and roadmap for in-plane and perpendicular STT-RAM,” in *IEEE Int. Memory Workshop*, May 2011, doi:10.1109/IMW.2011.5873205.
- [29] J. Slaughter *et al.*, “Fundamentals of MRAM technology,” *J. Superconductivity*, vol. 15, pp. 19–25, 2002, doi:10.1023/A:1014018925270.
- [30] J. Nahas *et al.*, “A 4Mb 0.18  $\mu$ m 1T1MTJ Toggle MRAM memory,” in *IEEE Int. Solid-State Circuits Conf.*, Feb. 2004, doi:10.1109/ISSCC.2004.1332585.
- [31] L. Savtchenko *et al.*, “Method of writing to scalable magnetoresistance random access memory element,” U.S. Patent 6 545 906, Apr. 8, 2003.
- [32] B.N. Engel *et al.*, “A 4-Mb toggle MRAM based on a novel bit and switching method,” *IEEE Trans. on Magnetics*, vol. 41, pp. 132–136, Jan. 2005, doi:10.1109/TMAG.2004.840847.
- [33] E. Technologies, “Toggle MRAM commercial products from Ever-spin technologies,” accessed in Nov. 2017, <https://www.everspin.com/toggle-mram-technology>.
- [34] H. Cai *et al.*, “High performance MRAM with spin-transfer-torque and voltage-controlled magnetic anisotropy effects,” *Applied Sciences*, vol. 7, p. 929, 2017, doi:10.3390/app7090929.
- [35] L. Berger, “Emission of spin waves by a magnetic multilayer traversed by a current,” *Phys. Rev. B*, vol. 54, pp. 9353–9358, Oct. 1996, doi:10.1103/PhysRevB.54.9353.
- [36] J. Slonczewski, “Current-driven excitation of magnetic multilayers,” *Journal of Magnetism and Magnetic Materials*, vol. 159, pp. L1–L7, 1996, doi:10.1016/0304-8853(96)00062-5.
- [37] J. Sun, “Spin-current interaction with a monodomain magnetic body: A model study,” *Phys. Rev. B*, vol. 62, pp. 570–578, 2000, doi:10.1103/PhysRevB.62.570.
- [38] A. Aharoni, “Micromagnetics: past, present and future,” *Physica B: Condensed Matter*, vol. 306, pp. 1–9, 2001, doi:10.1016/S0921-4526(01)00954-1.
- [39] R.H. Koch, J.A. Katine, and J.Z. Sun, “Time-resolved reversal of spin-transfer switching in a nanomagnet,” *Phys. Rev. Lett.*, vol. 92, p. 088302, Feb. 2004, doi:10.1103/PhysRevLett.92.088302.
- [40] W.H. Butler *et al.*, “Switching distributions for perpendicular spin-torque devices within the macrospin approximation,” *Trans. Magnetics*, vol. 48, pp. 4684–4700, Dec. 2012, doi:10.1109/TMAG.2012.2209122.
- [41] D. Bedau *et al.*, “Spin-transfer pulse switching: From the dynamic to the thermally activated regime,” *Appl. Phys. Lett.*, vol. 97, p. 262502, 2010, doi:10.1063/1.3532960.
- [42] E.B. Myers *et al.*, “Thermally activated magnetic reversal induced by a spin-polarized current,” *Phys. Rev. Lett.*, vol. 89, p. 196801, Oct. 2002, doi:10.1103/PhysRevLett.89.196801.
- [43] S. Van Beek *et al.*, “Impact of processing and stack optimization on the reliability of perpendicular STT-MRAM,” in *IEEE International Reliability Physics Symposium*, 2017, doi:10.1109/IRPS.2017.7936318.
- [44] A.A. Khan *et al.*, “Dielectric breakdown in Co-Fe-B/MgO/Co-Fe-B magnetic tunnel junction,” *Journal of Applied Physics*, vol. 103, 2008, doi:10.1063/1.2939571.
- [45] C. Yoshida *et al.*, “A study of dielectric breakdown mechanism in CoFeB/MgO/CoFeB magnetic tunnel junction,” *IEEE Int. Reliability Physics Symp.*, pp. 139–142, 2009, doi:10.1109/IRPS.2009.5173239.
- [46] M. Schäfers *et al.*, “Electric breakdown in ultrathin MgO tunnel barrier junctions for spin-transfer torque switching,” *Appl. Phys. Lett.*, vol. 95, pp. 1–4, 2009, doi:10.1063/1.3272268.
- [47] A.A. Khan, “Analysis of dielectric breakdown in CoFeB/MgO/CoFeB magnetic tunnel junction,” *Microelectronics Reliability*, vol. 55, pp. 894–902, 2015, doi:10.1016/j.microrel.2015.02.018.
- [48] J. Kim *et al.*, “Spin-Hall effect MRAM based cache memory: A feasibility study,” in *Device Research Conference*, Jun. 2015, doi:10.1109/DRC.2015.7175583.
- [49] Y. Kim, S.H. Choday, and K. Roy, “DSH-MRAM: Differential spin hall MRAM for on-chip memories,” *IEEE Electron Device Letters*, vol. 34, pp. 1259–1261, 2013, doi:10.1109/LED.2013.2279153.
- [50] B.K. Kaushik *et al.*, “Next generation spin torque memories,” *SpringerBriefs in Applied Sciences and Technology*, pp. i–iv, 2017, doi:10.1007/978-981-10-2720-8.
- [51] M.H. Tsai *et al.*, “Spin-orbit-torque MRAM: from uniaxial to unidirectional switching,” Jun. 2017, <https://arxiv.org/abs/1706.01639>.
- [52] H. Yoda *et al.*, “Voltage-control spintronics memory (VoCSM) having potentials of ultra-low energy-consumption and high-density,” in *IEEE Int. Electron Devices Meeting*, Dec. 2016, doi:10.1109/IEDM.2016.7838495.
- [53] J.M. Hu *et al.*, “Design of a voltage-controlled magnetic random access memory based on anisotropic magnetoresistance in a single magnetic layer,” *Advanced Materials*, vol. 24, pp. 2869–2873, 2012, doi:10.1002/adma.201201004.
- [54] MRAM-info, “GlobalFoundries: 22nm eMRAM technology is now available, prototyping to start in Q1 2018,” accessed in Sep. 2017, <https://www.mram-info.com/globalfoundries-22nm-emram-technology-now-available-prototyping-start-q1-2018>.
- [55] C.J. Lin *et al.*, “45nm low power CMOS logic compatible embedded STT MRAM utilizing a reverse-connection 1T/1MTJ cell,” in *IEEE Int. Electron Devices Meeting*, Dec. 2009, doi:10.1109/IEDM.2009.5424368.
- [56] Y.M. Lee *et al.*, “Highly scalable STT-MRAM with MTJs of top-pinned structure in 1T/1MTJ Cell,” in *Symp. VLSI Technology*, 2010, doi:10.1109/VLSIT.2010.5556123.
- [57] D. Lee, S.K. Gupta, and K. Roy, “High-performance low-energy STT MRAM based on balanced write scheme,” in *ACM/IEEE Int. Symp. Low Power Electronics and Design*, 2012, doi:10.1145/2333660.2333665.
- [58] A.K. Jones *et al.*, “Asymmetry of MTJ switching and its implication to STT-RAM designs,” in *Design, Automation and Test in Europe*, 2012, doi:10.1109/DATE.2012.6176695.
- [59] W. Zhao *et al.*, “Design considerations and strategies for high-reliable STT-MRAM,” *Microelectronics Reliability*, vol. 51, pp. 1454–1458, 2011, doi:10.1016/j.microrel.2011.07.001.
- [60] S. Hamdioui and A. Van De Goor, “An experimental analysis of spot defects in SRAMs: realistic fault models and tests,” in *Asian Test Symposium*, 2000, doi:10.1109/ATS.2000.893615.
- [61] Y.J. Song *et al.*, “Highly functional and reliable 8Mb STT-MRAM embedded in 28nm logic,” in *IEEE Int. Electron Devices Meeting*, 2016, doi:10.1109/IEDM.2016.7838491.
- [62] M. Bushnell and V.D. Agrawal, *Essentials of Electronic Testing for Digital, Memory and Mixed-Signal VLSI Circuits*. Springer Science & Business Media, 2004, vol. 30, <http://read.pudn.com/downloads111/ebook/464012/Essentials%20of%20Electronic%20Testing%20for%20Digital%20Memory%20and%20Mixed%20Signal%20VLSI%20Circuits.pdf>.
- [63] L. Tillie *et al.*, “Data retention extraction methodology for perpendicular STT-MRAM,” in *IEEE Int. Electron Devices Meeting*, 2016, doi:10.1109/IEDM.2016.7838492.
- [64] D. Shum *et al.*, “CMOS-embedded STT-MRAM arrays in 2x nm nodes for GP-MCU applications,” in *Symp. VLSI Technology*, Jun. 2017, doi:10.23919/VLSIT.2017.7998174.
- [65] W. Zhao *et al.*, “Failure analysis in magnetic tunnel junction nanopillar with interfacial perpendicular magnetic anisotropy,” *Materials*, vol. 9, pp. 1–17, 2016, doi:10.3390/ma9010041.
- [66] Y.G. Fedorenko, “Ion-beam-induced defects in CMOS technology: methods of study,” *arXiv:1701.07087*, 2017, doi:10.5772/67760.
- [67] F. Beenker, R. Bennetts, and A. Thijssen, “Defect-oriented testing,” in *Testability Concepts for Digital ICs. Frontiers in Electronic Testing*. Springer, 1995, vol. 3.
- [68] M. Sachdev and J.P. de Gyvez, *Defect-oriented testing for nano-metric CMOS VLSI circuits*. Springer Science & Business Media, 2007.
- [69] and E. J. McCluskey, “Diagnosis of resistive-open and stuck-open defects in digital CMOS ICs,” *IEEE Trans. Computer-Aided Design of Integrated Circuits and Systems*, vol. 24, pp. 1748–1759, Nov. 2005, doi:10.1109/TCAD.2005.852457.
- [70] N.Z. Haron and S. Hamdioui, “On defect oriented testing for hybrid CMOS/Memristor memory,” in *Asian Test Symp.*, Nov. 2011, doi:10.1109/ATS.2011.66.
- [71] G.S. Kar *et al.*, “Co/Ni based p-MTJ stack for sub-20nm high density stand alone and high performance embedded memory application,” in *IEEE Int. Electron Devices Meeting*, Dec. 2014, doi:10.1109/IEDM.2014.7047080.

- [72] E.I. Vatajelu *et al.*, "Challenges and solutions in emerging memory testing," *IEEE Trans. Emerging Topics in Computing*, pp. 1–1, Apr. 2017, doi:10.1109/TETC.2017.2691263.
- [73] M. Komalan *et al.*, "Cross-layer design and analysis of a low power, high density STT-MRAM for embedded systems," in *IEEE Int. Symp. Circuits and Systems*, May 2017, doi:10.1109/ISCAS.2017.8050923.
- [74] B. Oliver *et al.*, "Two breakdown mechanisms in ultrathin alumina barrier magnetic tunnel junctions," *Journal of Applied Physics*, vol. 95, pp. 1315–1322, 2004, doi:10.1063/1.1636255.
- [75] K. Sugiura *et al.*, "Ion beam etching technology for high-density spin transfer torque magnetic random access memory," *Japanese Journal of Applied Physics*, vol. 48, 2009, doi:10.1143/JJAP.48.08HD02.
- [76] H. Meng *et al.*, "Annealing effects on CoFeB-MgO magnetic tunnel junctions with perpendicular anisotropy," *J. Appl. Phys.*, vol. 110, p. 033904, 2011, doi:10.1063/1.3611426.
- [77] H. Maehara *et al.*, "Tunnel magnetoresistance above 170% and resistance-area product of  $1 \Omega (\mu\text{m})^2$  attained by in situ annealing of ultrathin MgO tunnel barrier," *Applied Physics Express*, vol. 4, p. 033002, Mar. 2011, doi:10.1143/apex.4.033002.
- [78] B. Bhusan Singh and S. Chaudhary, "Effect of MgO spacer and annealing on interface and magnetic properties of ion beam sputtered NiFe/Mg/MgO/CoFe layer structures," *J. Appl. Phys.*, vol. 112, p. 063906, 2012, doi:10.1063/1.4752264.
- [79] J.G. Park *et al.*, "Challenging issues for terra-bit-level perpendicular STT-MRAM," in *IEEE Int. Electron Devices Meeting*, Dec. 2014, doi:10.1109/IEDM.2014.7047081.
- [80] W. Boullart *et al.*, "STT MRAM patterning challenges," in *Proc. SPIE 8685, Advanced Etch Technology for Nanopatterning II*, Mar. 2013, doi:10.1117/12.2013602.
- [81] K. Nagahara *et al.*, "Ion-beam-etched profile control of MTJ cells for improving the switching characteristics of high-density MRAM," *IEEE Trans. Magnetics*, vol. 42, pp. 2745–2747, 2006, doi:10.1109/TMAG.2006.878862.
- [82] K. Nagahara *et al.*, "Magnetic tunnel junction (MTJ) patterning for magnetic random access memory (MRAM) process applications," *Japanese Journal of Applied Physics*, vol. 42, 05 2003, doi:10.1143/JJAP.42.L499.
- [83] E.H. Kim, T.Y. Lee, and C.W. Chung, "Evolution of etch profile of magnetic tunnel junction stacks etched in a  $\text{CH}_3\text{OH}/\text{Ar}$  plasma," *J. Electrochemical Society*, vol. 159, pp. H230–H234, 2012, doi:10.1149/2.012203jes.
- [84] A.A. Garay *et al.*, "Inductively coupled plasma reactive ion etching of magnetic tunnel junction stacks in a  $\text{CH}_3\text{COOH}/\text{Ar}$  gas," *ECS Solid State Letters*, vol. 4, pp. P77–P79, 2015, doi:10.1149/2.0071510ssl.
- [85] J.H. Jeong and T. Endoh, "Novel oxygen showering process (OSP) for extreme damage suppression of sub-20nm high density p-MTJ array without IBE treatment," in *Symp. VLSI Technology*, Jun. 2015, doi:10.1109/VLSIT.2015.7223660.
- [86] K. Lee *et al.*, "22-nm FD-SOI embedded MRAM with full solder reflow compatibility and enhanced magnetic immunity," in *IEEE Symp. VLSI Technology*, Jun. 2018, doi:10.1109/VLSIT.2018.8510655.
- [87] W. Kang *et al.*, "Yield and reliability improvement techniques for emerging nonvolatile STT-MRAM," *IEEE Journal on Emerging and Selected Topics in Circuits and Systems*, vol. 5, pp. 28–39, 2015, doi:10.1109/JETCAS.2014.2374291.
- [88] A. Chintaluri *et al.*, "Analysis of defects and variations in embedded spin transfer torque (STT) MRAM arrays," *IEEE Journal on Emerging and Selected Topics in Circuits and Systems*, vol. 6, pp. 319–329, 2016, doi:10.1109/JETCAS.2016.2547779.
- [89] W. Kang *et al.*, "Reconfigurable codesign of STT-MRAM under process variations in deeply scaled technology," *IEEE Trans. Electron Devices*, vol. 62, pp. 1769–1777, 2015, doi:10.1109/ED.2015.2412960.
- [90] Y. Ye *et al.*, "Statistical modeling and simulation of threshold variation under random dopant fluctuations and line-edge roughness," *IEEE Trans. VLSI Systems*, vol. 19, pp. 987–996, Jun. 2011, doi:10.1109/TVLSI.2010.2043694.
- [91] W. Zhao and Y. Cao, "Predictive technology model for nano-CMOS design exploration," *J. Emerg. Technol. Comput. Syst.*, vol. 3, Apr. 2007, doi:10.1145/1229175.1229176.
- [92] Y. Wang *et al.*, "Impact of stray field on the switching properties of perpendicular MTJ for scaled MRAM," in *IEEE Int. Electron Devices Meeting*, Dec. 2012, doi:10.1109/IEDM.2012.6479127.
- [93] C. Augustine *et al.*, "Numerical analysis of typical STT-MTJ stacks for 1T-1R memory arrays," *Int. Electron Devices Meeting*, 2010, doi:10.1109/IEDM.2010.5703416.
- [94] S. Bandiera *et al.*, "Comparison of synthetic antiferromagnets and hard ferromagnets as reference layer in magnetic tunnel junctions with perpendicular magnetic anisotropy," *IEEE Magnetics Letters*, vol. 1, pp. 1–4, 2010, doi:10.1109/LMAG.2010.2052238.
- [95] L. Xue *et al.*, "A self-aligned two-step reactive ion etching process for nanopatterning magnetic tunnel junctions on 300 mm Wafers," *IEEE Trans. Magnetics*, vol. 50, pp. 10–12, 2014, doi:10.1109/TMAG.2014.2322351.
- [96] I. Yoon, A. Chintaluri, and A. Raychowdhury, "EMACS: Efficient MBIST architecture for test and characterization of STT-MRAM arrays," in *IEEE Int. Test Conf.*, Nov. 2016, doi:10.1109/TEST.2016.7805834.
- [97] I. Yoon and A. Raychowdhury, "Modeling and analysis of magnetic field induced coupling on embedded STT-MRAM arrays," *IEEE Transactions on Computer-Aided Design of Integrated Circuits and Systems*, vol. 37, pp. 337–349, 2018, doi:10.1109/TCAD.2017.2697963.
- [98] W. Zhao *et al.*, "Failure and reliability analysis of STT-MRAM," *Microelectronics Reliability*, vol. 52, pp. 1848–1852, 2012, doi:10.1016/j.microrel.2012.06.035.
- [99] T. Devolder *et al.*, "Single-shot time-resolved measurements of nanosecond-scale spin-transfer induced switching: stochastic versus deterministic aspects," *Physical Review Letters*, vol. 100, 2008, doi:10.1103/PhysRevLett.100.057206.
- [100] M. Marins De Castro *et al.*, "Precessional spin-transfer switching in a magnetic tunnel junction with a synthetic antiferromagnetic perpendicular polarizer," *J. Appl. Phys.*, vol. 111, 2012, doi:10.1063/1.3676610.
- [101] K. Roy, "Beyond charge-based computing," in *Asia and South Pacific Design Auto. Conf.*, 2014, <http://www.aspdac.com/aspdac2014/keynote/Roy-ASP-DAC-Keynote2014.pdf>.
- [102] B. Wu *et al.*, "Temperature impact analysis and access reliability enhancement for 1T1MTJ STT-RAM," *IEEE Trans. Reliability*, vol. 65, pp. 1755–1768, Dec. 2016, doi:10.1109/TR.2016.2608910.
- [103] X. Wang *et al.*, "Thermal fluctuation effects on spin torque induced switching: mean and variations," *J. Appl. Phys.*, vol. 103, 2008, doi:10.1063/1.2837800.
- [104] J.C. Sankey *et al.*, "Measurement of the spin-transfer-torque vector in magnetic tunnel junctions," *Nature Physics*, vol. 4, pp. 67–71, 2008, doi:10.1038/nphys783.
- [105] W. Kang *et al.*, "Pds: pseudo-differential sensing scheme for stt-mram," in *ACM Proc. Design Auto. Conf.*, 2016, doi:10.1145/2897937.2898058.
- [106] L. Faber *et al.*, "Dynamic compact model of spin-transfer torque based magnetic tunnel junction (MTJ)," in *Int. Conf. Design Technology of Integrated Systems in Nanoscale Era*, Apr. 2009, doi:10.1109/DTIS.2009.4938040.
- [107] C. Augustine *et al.*, "Design space exploration of typical STT MTJ stacks in memory arrays in the presence of variability and disturbances," *IEEE Trans. Electron Devices*, vol. 58, pp. 4333–4343, 2011, doi:10.1109/TED.2011.2169962.
- [108] X. Kou *et al.*, "Temperature dependence of the resistance of magnetic tunnel junctions with MgO barrier," *Appl. Phys. Lett.*, vol. 88, pp. 1–4, 2006, doi:10.1063/1.2206680.
- [109] H. Zhao *et al.*, "Spin-transfer torque switching above ambient temperature," *IEEE Magnetics Letters*, vol. 3, pp. 3 000 304–3 000 304, 2012, doi:10.1109/LMAG.2012.2195775.
- [110] L. Zhang *et al.*, "Reliability and performance evaluation for stt-mram under temperature variation," in *Int. Conf. Thermal, Mech. and Multi-Phys. Simul. and Exp. in Microelectronics and Microsystems (EuroSimE)*, Apr. 2016, doi:10.1109/EuroSimE.2016.7463380.
- [111] K. Lee and S.H. Kang, "Design consideration of magnetic tunnel junctions for reliable high-temperature operation of STT-MRAM," *IEEE Trans. Magnetics*, vol. 46, pp. 1537–1540, Jun. 2010, doi:10.1109/TMAG.2010.2043645.
- [112] I.L. Prejbeanu *et al.*, "Thermally assisted MRAM," *J. Phys.: Condensed Matter*, vol. 19, p. 165218, Apr. 2007, doi:10.1088/0953-8984/19/16/165218.
- [113] S. Chaudhuri *et al.*, "Design of TAS-MRAM prototype for NV embedded memory applications," in *IEEE Int. Memory Workshop*, May 2010, doi:10.1109/IMW.2010.5488401.
- [114] S.M. Nair *et al.*, "Defect injection, fault modeling and test algorithm generation methodology for STT-MRAM," in *IEEE Int. Test Conf.*, Oct. 2018, doi:10.1109/TEST.2018.8624725.
- [115] and J. H. Jeong *et al.*, "Extended scalability of perpendicular stt-mram towards sub-20nm mtj node," in *IEEE Int. Electron Devices Meeting*, Dec. 2011, doi:10.1109/IEDM.2011.6131602.
- [116] A. Raychowdhury *et al.*, "Design space and scalability exploration of 1T-1STT MTJ memory arrays in the presence of variability and disturbances," in *IEEE Int. Electron Devices Meeting*, Dec. 2009, doi:10.1109/IEDM.2009.5424242.

- [117] X. Fong *et al.*, “Failure mitigation techniques for 1T-1MTJ spin-transfer torque MRAM bit-cells,” *IEEE Trans. VLSI Systems*, vol. 22, pp. 384–395, Feb. 2014, doi:10.1109/TVLSI.2013.2239671.
- [118] Y. Zhang *et al.*, “STT-RAM cell optimization considering MTJ and CMOS variations,” *IEEE Trans. Magnetics*, vol. 47, pp. 2962–2965, 2011, doi:10.1109/TMAG.2011.2158810.
- [119] D. Apalkov *et al.*, “Spin-transfer torque magnetic random access memory (STT-MRAM),” *J. Emerg. Technol. Comput. Syst.*, vol. 9, pp. 13:1–13:35, May 2013, doi:10.1145/2463585.2463589.
- [120] R. Bishnoi *et al.*, “Read disturb fault detection in STT-MRAM,” in *Int. Test Conf.*, Oct. 2014, doi:10.1109/TEST.2014.7035342.
- [121] Y. Ran *et al.*, “Read disturbance issue and design techniques for nanoscale STT-MRAM,” *Journal of Systems Architecture*, vol. 71, pp. 2–11, 2016, doi:10.1016/j.sysarc.2016.05.005.
- [122] H. Naeimi *et al.*, “STTRAM scaling and retention failure,” *Intel Technology Journal*, vol. 17, 2013, <https://www.intel.com/content/dam/www/public/us/en/documents/research/2013-vol17-iss-1\intel-technology-journal.pdf#page=54>.
- [123] R. Heindl *et al.*, “Validity of the thermal activation model for spin-transfer torque switching in magnetic tunnel junctions,” *Journal of Applied Physics*, vol. 109, 2011, doi:10.1063/1.3562136.
- [124] A. Iyengar, S. Ghosh, and S. Srinivasan, “Retention testing methodology for STTRAM,” *IEEE Design & Test*, vol. 33, pp. 7–15, 2016, doi:10.1109/MDAT.2016.2591554.
- [125] C.L. Su *et al.*, “MRAM defect analysis and fault modeling,” in *Int. Test Conf.*, Oct. 2004, doi:10.1109/TEST.2004.1386944.
- [126] C. Su *et al.*, “Testing MRAM for write disturbance fault,” in *IEEE Int. Test Conf.*, Oct. 2006, doi:10.1109/TEST.2006.297702.
- [127] C.W. Smullen *et al.*, “Relaxing non-volatility for fast and energy-efficient STT-RAM caches,” in *IEEE Int. Symp. High Performance Computer Architecture*, Feb. 2011, doi:10.1109/HPCA.2011.5749716.
- [128] J. Li *et al.*, “Low-energy volatile STT-RAM cache design using cache-coherence-enabled adaptive refresh,” *ACM Trans. Des. Autom. Electron. Syst.*, vol. 19, pp. 5:1–5:23, Dec. 2013, doi:10.1145/2534393.
- [129] Z. Sun *et al.*, “STT-RAM cache hierarchy with multiretention MTJ designs,” *IEEE Trans. Very Large Scale Integration Systems*, vol. 22, pp. 1281–1293, Jun. 2014, doi:10.1109/TVLSI.2013.2267754.
- [130] I. Yoon and A. Raychowdhury, “Test challenges in embedded STT-MRAM arrays,” in *Int. Symp. Quality Electronic Design*, Mar. 2017, doi:10.1109/ISQED.2017.7918289.
- [131] L. Wu *et al.*, “Pinhole defect characterization and fault modeling for STT-MRAM testing,” in *European Test Symp.*, May 2019, doi:10.1109/ETS.2019.8791518.
- [132] L. Wu *et al.*, “Electrical modeling of STT-MRAM defects,” in *IEEE Int. Test Conf.*, Oct. 2018, doi:10.1109/TEST.2018.8624749.
- [133] G. Han *et al.*, “Control of offset field and pinning stability in perpendicular magnetic tunnelling junctions with synthetic antiferromagnetic coupling multilayer,” *J. Appl. Phys.*, vol. 117, p. 17B515, 2015, doi:10.1063/1.4913942.
- [134] D. Saida *et al.*, “Sub-3 ns pulse with sub-100  $\mu$ A switching of 1x2x nm perpendicular MTJ for high-performance embedded STT-MRAM towards sub-20 nm CMOS,” in *IEEE Symp. VLSI Technology*, Jun. 2016, doi:10.1109/VLSIT.2016.7573412.
- [135] L. Wu *et al.*, “Defect and Fault Modeling Framework for STT-MRAM Testing,” in *IEEE Trans. Emerging Topics in Computing*, Dec. 2019, doi:10.1109/TETC.2019.2960375.
- [136] S. Hamdioui *et al.*, “Dynamic faults in random-access-memories: concept, fault models and tests,” *J. Electronic Testing*, vol. 19, pp. 195–205, 2003, doi:10.1023/A:1022802010738.